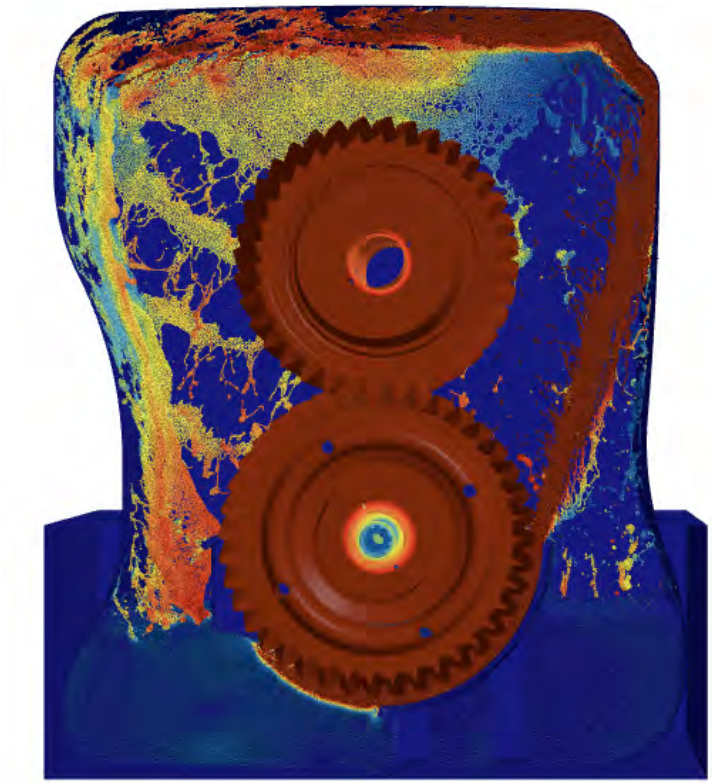


Transmission housing influence on gear churning losses

A Master's Thesis in Mobility Engineering

Mobility Engineering

KEVIN CHRISTOFORIDIS JOHANSSON

DEPARTMENT OF MECHANICS AND MARITIME SCIENCES

CHALMERS UNIVERSITY OF TECHNOLOGY
Gothenburg, Sweden 2026
www.chalmers.se

Master's thesis 2026

Transmission housing influence on gear churning losses

A Master's Thesis in Mobility Engineering

Kevin Christoforidis Johansson



CHALMERS
UNIVERSITY OF TECHNOLOGY

Department of Mechanics and Maritime Sciences
Division of Fluid Dynamics
Chalmers University of Technology
Gothenburg, Sweden 2026

Transmission housing influence on gear churning losses
A Master's Thesis in Mobility Engineering
KEVIN CHRISTOFORIDIS JOHANSSON

© KEVIN CHRISTOFORIDIS JOHANSSON, 2026.

Supervisor: Robert Johansson, Volvo AB, Powertrain Technology, Driveline (BE83640, Oil, Clutch and Retarder Systems)
Examiner: Valery Chernoray, Division of Fluid Dynamics

Master's Thesis 2026
Department of Mechanics and Maritime Sciences
Division of Fluid Dynamics
Chalmers University of Technology
SE-412 96 Gothenburg
Telephone +46 31 772 1000

Cover: Oil splashing visualized from a CFD simulation.

Typeset in LaTeX
Printed by Chalmers Reproservice
Gothenburg, Sweden 2026

Transmission housing influence on gear churning losses
A Master's Thesis in Mobility Engineering
KEVIN CHRISTOFORIDIS JOHANSSON
Department of Mechanics and Maritime Sciences
Chalmers University of Technology

Abstract

With stricter emission regulations from the European Union, there is an increasing need for more efficient heavy-duty transport solutions. Around 5.1% of wasted fuel energy stems from transmission losses in internal combustion-driven heavy-duty vehicles. For electric vehicles, transmission efficiency is even more important due to the higher efficiency of the motor compared to ICEs. This thesis investigates how transmission housing design can reduce churning losses in Volvo's AMT dip-lubricated gearboxes, thereby improving overall efficiency and lowering emissions. These losses vary with speed and result from oil splashes within the transmission due to gear interaction. Using SPH simulations and an existing Chalmers test rig (with a vertical gear pair), the study focuses on how the interaction between gears, lubrication oil and housing geometry influences these losses. The housing geometry is modified using CAD-designed insertions to change the flow behavior within the transmission. As simulation and experimental data are gathered, a comparison is made to evaluate the level of agreement between the two. The findings suggest that there are substantial efficiency gains to be had, especially when insertion geometries that utilize axial walls around the lower gear are used. The results also show that the insertions altered the oil flow and forced different recirculation paths in the sump, which might help minimize losses. However, it was found that the simulated power loss values and overall flow did not match the experimental results. This would indicate that the single-phase model used is insufficient and the results could only be used qualitatively to study recirculation in the sump.

Keywords: Churning losses, Load independent, SPH, Simulation, Testing, Test rig, Experimental, Splash losses, Power losses

Acknowledgements

I want to thank my supervisors, Robert Johansson and Henrik Hagerman at Volvo TTI, for their continuous support and for providing me with a place to work and the necessary equipment to complete this thesis. Also, a special thanks to Rikard Graas and his team, who supported me with the test rig and provided CAD files. I also want to thank my examiner, Valery Chernoray, for taking responsibility for this thesis. This, in combination with the countless competent people at Volvo TTI. All of you have addressed any doubts and exceeded my expectations regarding project completion and interest in the success of my work. All this help has significantly improved the outcome of this thesis.
Lastly, I want to thank my family and friends for supporting me both in this project and during times when I had to be elsewhere to represent Sweden in Ju-Jitsu Fighting.

Kevin Christoforidis Johansson, Gothenburg, June 2026

List of Acronyms

Below is the list of acronyms that have been used throughout this thesis listed in alphabetical order:

AMT	Automated Manual Transmission
BEV	Battery Electric Vehicle
CAD	Computer Aided Design
CFD	Computational Fluid Dynamics
FA	Full Axial
FVM	Finite Volume Method
FR	Full Radial
FZG	Forschungsstelle für Zahnräder und Getriebebau
HA	Half Axial
HR	Half Radial
ICE	Internal Combustion Engine
REF	Reference
RPM	Revolutions Per Minute
SPH	Smoothed Particle Hydrodynamics
TTI	Volvo Group Trucks Technology & Industrial Division

Nomenclature

Below is the nomenclature of indices and variables that have been used throughout this thesis.

Indices

i	Numbered index

Variables

P_{LGO}	Total load independent power loss
$P_{LGO,C}$	Churning power loss
$P_{LGO,S}$	Squeezing power loss
$P_{LGO,W}$	Windage power loss
s	Standard deviation
S	Seebeck coefficient
$\bar{x}$	Measurement mean
x_i	Measurement value
N	Total number of measurements
ω	Rotational speed [Rad/s]
n	Rotational speed [RPM]
f	Frequency [Hz]
Z	Number of teeth on a gear
T_{hot}	Oil temperature/hot side of thermocouple
T_{ref}	Reference temperature of thermocouple

Contents

List of Acronyms **ix**

Nomenclature **xi**

List of Figures **xvii**

List of Tables **xix**

1 Introduction **1**
1.1 Background . . . 1
1.2 Purpose . . . 2
1.3 Previous studies . . . 3
1.3.1 Experimental Investigation . . . 3
1.3.2 A comparative study on oil flow and bubble distribution . . . 3
1.3.3 Study of Fluid Flow Inside The Gearbox . . . 4
1.3.4 Housing Influence on Churning Losses in Geared Transmissions 4
1.3.5 Key takeaways . . . 6
1.4 Aim . . . 6
1.5 Demarcations . . . 6
1.6 Social, ethical and ecological aspects . . . 7

2 Theory **9**
2.1 Basic transmission operation . . . 9
2.2 Load independent losses . . . 10
2.3 Oil aeration . . . 11
2.4 Measurement uncertainties . . . 12
2.5 Smooth Particle Hydrodynamics . . . 12

3 Methods **15**
3.1 CAD and prototyping . . . 15
3.2 SPH simulation . . . 16
3.3 Test rig testing . . . 16

4 CAD and prototyping **17**
4.1 Design process . . . 17
4.1.1 Concept matrix . . . 17
4.1.2 Sketching . . . 19

4.1.3 Half axial + Half radial . . . 20
4.1.4 Half axial + Full radial . . . 20
4.1.5 Full axial + Half radial . . . 21
4.1.6 No axial + Full radial . . . 22
4.1.7 No axial + Half radial . . . 22
4.1.8 Insertion mounting . . . 23
4.1.8.1 Final mounting concept . . . 24
4.1.9 Modifications before 3D printing . . . 25
4.2 Selected designs for SPH . . . 26

5 SPH simulation 27
5.1 Pre-processing . . . 27
5.1.1 Bounded box . . . 27
5.1.1.1 Surface models . . . 28
5.1.2 Physics . . . 29
5.2 Simulation conditions . . . 30

6 Test rig testing 33
6.1 Test rig setup . . . 33
6.1.1 Oil level . . . 33
6.1.2 Oil type . . . 34
6.1.3 Sensors . . . 34
6.1.3.1 Torque sensor . . . 34
6.1.3.2 Speed sensor . . . 35
6.1.3.3 Temperature sensor . . . 35
6.2 Testing plan . . . 36

7 Results 37
7.1 SPH simulation . . . 37
7.1.1 Simulation plots . . . 37
7.1.2 Relative performance comparison . . . 38
7.1.3 Oil flow . . . 39
7.1.3.1 Recirculation . . . 42
7.2 Test rig testing . . . 44
7.2.1 Flow observations . . . 46
7.3 Simulation vs experimental results . . . 52

8 Discussion 53

Future work 57

Conclusion 58

Declaration of AI use 59

Bibliography 61

A CAD I

B Simulation and testing **III**
B.1 Simulation III
B.2 Testing IX

C Timeplan **XI**

List of Figures

1.1 Energy consumption of heavy duty ICE vehicles from [Holmberg et al., 2014] . . . 1
1.2 Visualization of the flow pattern, blue arrow indicates rotational direction of the top gear. Courtesy of [Opdam, 2023] . . . 3
1.3 Hartonos's FZG test setup, courtesy of [Hartono, 2014] . . . 4
1.4 3D assembly model of Chengnet and Velex test rig, courtesy of [Changenet and Velex, 2008] . . . 5
1.5 Axial clearance influence on losses, courtesy of [Changenet and Velex, 2008] . . . 5

2.1 Basic 5-speed manual transmission sketch . . . 9
2.2 Diagram of a Volvo AMT, courtesy of TTI . . . 10
2.3 Illustration of load independent losses based on a CFD simulation, courtesy of [Liu et al., 2018] . . . 11
2.4 2D example of how SPH particles can move, courtesy of [Dong et al., 2022] . . . 13
2.5 Two examples of kernel functions, courtesy of [DiveCAE, 2020] . . . 13

4.1 Sketches of the investigated configurations: (a) Half axial + Half radial, (b) Half axial + Full radial, (c) Full axial + Half radial, (d) No axial + Full radial, (e) No axial + Half radial. . . . 19
4.2 Half axial + Half radial in CAD . . . 20
4.3 Half axial + Full radial in CAD . . . 21
4.4 Full axial + Half radial in CAD . . . 21
4.5 No axial + Full radial in CAD . . . 22
4.6 No axial + half radial in CAD . . . 23
4.7 3D-model of test rig box with transmission housing, bottom part in blue and top part in gray, courtesy of [Fransson and Eliasson, 2021] . 23
4.8 Lower transmission housing with insertion, blue in figure . . . 24
4.9 Test rig box with lower housing geometry and insertion split . . . 25

5.1 Bounded box of transmission housing . . . 28
5.2 Surface models in STARCCM+: . . . 29

6.1 Oil level reference for lower gear . . . 33
6.2 Speed sensor . . . 35

7.1 Reference total power at 1200RPM . . . 38

7.2 Relative power simulation comparison, HA+HR vs REF 38
7.3 Relative power simulation comparison, FA+HR vs REF 39
7.4 REF velocity magnitude of oil flow at 1200RPM: 40
7.5 HA+HR velocity magnitude of oil flow at 1200RPM: 41
7.6 FA+HR velocity magnitude of oil flow at 1200RPM: 42
7.7 Oil flow recirculation of REF at 1200 RPM 43
7.8 Oil flow recirculation of HA+HR at 1200 RPM 43
7.9 Oil flow recirculation of FA+HR at 1200 RPM 44
7.10 Experimental relative power loss for all insertion concepts 45
7.11 REF oil flow at 600 RPM 46
7.12 FR oil flow at 600 RPM 47
7.13 HR (5mm and 10mm) oil flow at 600 RPM 48
7.14 HA+HR oil flow at 600 RPM 49
7.15 HA+FR oil flow at 600 RPM 50
7.16 FA+HR oil flow at 600 RPM 51

8.1 Hypothetical oil path or aerated oil: 55

A.1 Mounting concept where inserted geometry is separated from lower housing I
A.2 Divided parts of lower transmission housing: (a) Right wall, (b) Right empty plate, (c) Right radial insertion, (d) Right radial + axial insertion, (e) Left axial insertion, (f) Left radial insertion, (h) Left empty plate, (g) Left wall. II

B.1 REF velocity magnitude of oil flow at 1800RPM: IV
B.2 HA+HR velocity magnitude of oil flow at 1200RPM: V
B.3 FA+HR velocity magnitude of oil flow at 1200RPM: VI
B.4 Oil flow recirculation of REF at 1800 RPM VII
B.5 Oil flow recirculation of HA+HR at 1800 RPM VII
B.6 Oil flow recirculation of FA+HR at 1800 RPM VIII
B.7 Full test schematic IX

C.1 Gantt schedule XI

List of Tables

4.1 Concept Matrix 18
4.2 Concept Matrix with selected concepts 18

5.1 Physics Models 30
5.2 Simulation Configuration and Operational Conditions 31

6.1 97318/97307 Oil properties 34
6.2 Experimental Test Plan: RPM Sweep 36

7.1 Comparison of simulated and experimental power loss 52

1
Introduction

This chapter introduces the subject of this thesis. It presents the background to the problem, defines a clear purpose and aim of the study. The chapter also goes through limitations/demarcations of the project, previous studies in the subject and social/ecological/ethical aspects that the study touches upon.

1.1 Background

Transport is a big part of today's society and there is an increasing need for sustainable solutions to combat and slow down climate change. Heavy-duty transport vehicles are responsible for more than 6% of the EU's total greenhouse emissions [European Commission, 2023]. This in combination with constantly stricter emission regulations, puts an increasing demand on crucial components to be as efficient as possible while maintaining high reliability. The EU has a new proposal that is rapidly approaching by 2030. This proposal targets heavy-duty vehicles and aims to reduce CO_2 emissions by 45% compared to 2019. This targets the entire fleet average and not specific models [European Commission, 2023]. Volvo Group is constantly working to provide more sustainable solutions for customers. The aim is to provide them with zero-emission fleets by 2050 [Volvo Group, 2026]. However, internal combustion engines (ICE) will still play a big part in the future as well. An increasing need for sustainable fuels and minimizing losses is therefore of great importance.

Transmissions play a big part in overall vehicle efficiency/range and losses in these systems account for about 5.1 % of fuel energy used (see Figure 1.1):

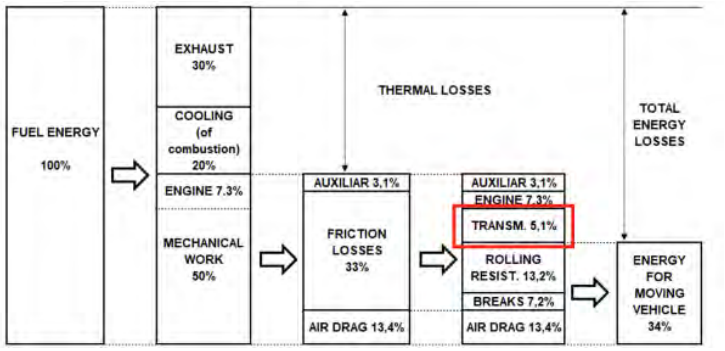


Figure 1.1: Energy consumption of heavy duty ICE vehicles from [Holmberg et al., 2014]

Minimizing transmission losses is therefore of interest and will have a real, measurable impact on both energy consumption and emissions. Especially for electric vehicles, as their motors operate with a higher efficiency than ICEs. This makes transmission efficiency gains more impactful. This will extend the range, which is always of interest for customers. Volvo Trucks has developed an Automated Manual Transmission (AMT) that is used in many of their ICE models and electric vehicles. [Volvo Trucks, 2026]. The project, therefore, affects both ICE and battery electric vehicles (BEV) that utilize a geared transmission.

Within the transmission, there are several different mechanisms that lead to losses. These can be categorized into load-dependent and load-independent losses. Load dependent losses come from friction that varies with load. This happens when surfaces come in mechanical contact with each other and move relatively. Load independent losses primarily come from fluid friction and vary with rotational speed. Examples of such losses are: windage losses, churning losses and squeezing/pocketing losses. In conventional gearboxes, lubrication is typically provided either by dip lubrication, where gears are partially immersed in an oil bath or by jet lubrication, where pressurized oil jets are directed towards the gear mesh and bearings [Hartono, 2019].

The main focus of this project is on churning losses from dip-lubrication. These losses occur due to the interaction between the lubrication oil, gears and housing geometry. Minimizing these losses while maintaining a reliable operating point for the gears is therefore a key challenge in transmission design.

1.2 Purpose

The objective of this master's thesis is to investigate how the interaction between transmission housing and gears influences churning losses in dip-lubricated transmissions. This will be achieved by isolating the problem and studying its effects using an existing Chalmers test rig in which the churning-loss issue has been isolated [Fransson and Eliasson, 2021]. Housing insertions will be designed using CAD, printed and tested to obtain empirical results from the rig. Insertion meaning the modified geometry that will be placed into the test rig.

The project will also include a simulation component using SPH (Smoothed Particle Hydrodynamics), with the aim of linking experimental data with simulation data and vice versa. This ensures that simulation results can be trusted in further rapid testing of different housing geometries. If time allows, there will also be a part focusing on how the housing geometry affects the cooling performance of the gears.

The results are expected to improve the knowledge on how different gearbox housing geometries affect transmission churning losses, contribute to future development of efficient gearboxes, and help the Volvo Group's climate strategy to reduce emissions in its fleet [Volvo Group, 2026].

1.3 Previous studies

Several previous studies have touched on related topics with regard to churning losses and flow around gears in different testing configurations. This section presents and assesses these studies.

1.3.1 Experimental Investigation

A study done by Wout Opdam [Opdam, 2023] focused on conducting experiments on how a new gear design at Volvo Trucks affected the load-independent churning losses in a gearbox. The same test rig as this study was used to compare the different gear designs, making the observations highly interesting. The first discussion point to note was how bubbles in the oil affect the churning losses. It was discussed that the bubbles in the oil have a dampening effect and would, in theory, increase the required energy to move the fluid. This in turn, would increase the churning losses as a result. The study also showed how aerated oil increased losses (5-9%) compared to non-aerated oil. Something that could be explained by the change in viscosity of the fluid.

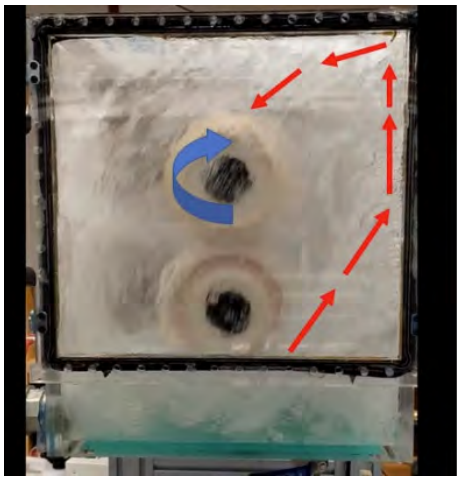


Figure 1.2: Visualization of the flow pattern, blue arrow indicates rotational direction of the top gear. Courtesy of [Opdam, 2023]

One of the most interesting observations in Opdam's study was the visualization of the flow pattern seen in Figure 1.2. It was noted that the splash direction (red arrows) of the flow was not favorable from a mechanical standpoint. As seen in the figure, the splash would in theory, yield opposing torque to the rotational direction of the top gear. Opdam therefore declared that it would seem worthwhile to investigate how different wall profiles could result in more favorable splash patterns.

1.3.2 A comparative study on oil flow and bubble distribution

A study conducted by Shao et al.., focused on visualizing and characterizing the oil flow and bubble distribution of an FZG gear pair simulated with SPH [Shao et al., 2026].

It was revealed that the bubbles in the oil (either from aerated oil or air mixed in the existing oil) acted as non-lubricating components that altered the flow characteristics of the oil and introduced additional instabilities and turbulence. This resulted in increased power losses that could be derived from increases in heat due to poorer lubricating characteristics. This observation would indicate that it is reasonable to introduce oil guide plates around gears to help minimize churning losses by reducing bubbles.

1.3.3 Study of Fluid Flow Inside The Gearbox

A study conducted by Erwin Adi Hartono focused on how the oil flow inside a simplified gearbox is distributed with the help of particle image velocimetry (PIV) and flash photography [Hartono, 2014]. The study was done on an FZG rig (see Figure 1.3).



Figure 1.3: Hartonos's FZG test setup, courtesy of [Hartono, 2014]

It was revealed that the flow is dominated by the recirculation region and that the cause of losses is probably due to strong recirculation. The study also observed how aerated oil gave an increased torque loss reading, in line with statements made in Shao et al's study (subsection 1.3.2). The conclusions of this work made statements regarding what future work should focus on. This includes the geometry of the transmission housing, which was said to influence the churning losses. By altering the geometry, the flow can be guided and redirected to a more favorable spot.

1.3.4 Housing Influence on Churning Losses in Geared Transmissions

In a similar study conducted by C. Chanenet and P. Velex, focused on how housing influences churning losses in a geared transmission [Changenet and Velex, 2008]. The study was done experimentally on and FZG test rig, where different factors of the housing was changed between tests. Below is a 3D assembly model in CAD of the test rig used (Figure 1.4):

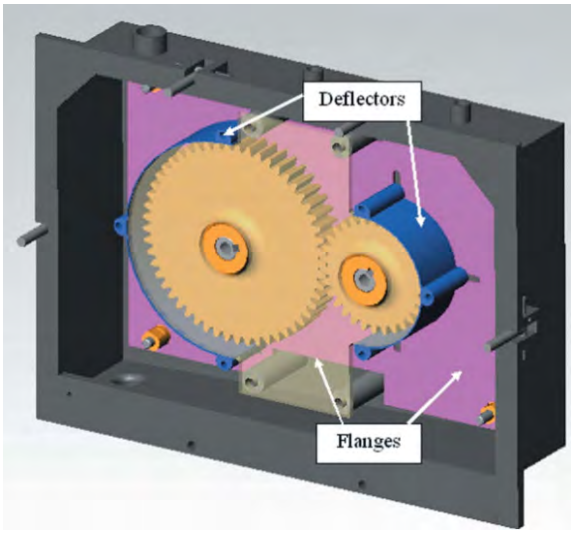


Figure 1.4: 3D assembly model of Chengnet and Velex test rig, courtesy of [Changenet and Velex, 2008]

The main factors of interest that were changed, were the radial and axial distances from the gears. The axial distance is shown in the figure above and is defined as the distance between the gear and the "Flanges". The radial distance is defined by the distance between the gear tip and the "Deflectors". It is important to note that the gear pair used in this study employed straight-cut gears. Unlike the previous studies above, this study found results that favored the axial distance over radial geometry. The churning losses were said to be almost insensitive to radial clearance and the losses were greatly reduced when axial clearance decreased from 7mm to 1mm. The figure below is taken from the study and shows these results (Figure 1.5):

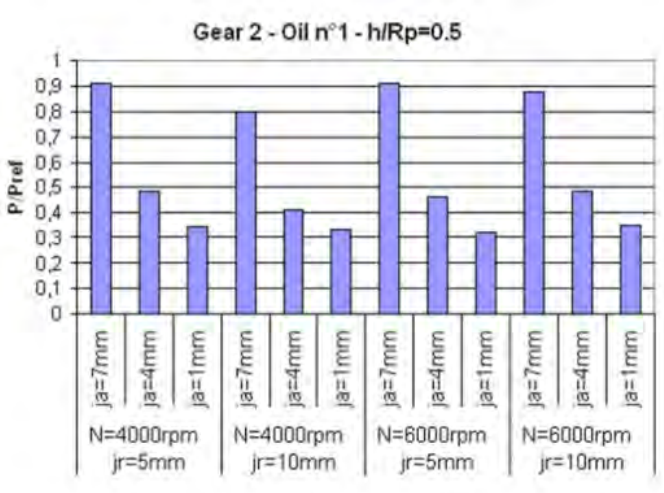


Figure 1.5: Axial clearance influence on losses, courtesy of [Changenet and Velex, 2008]

As shown in the figure, the y-axis represents the losses compared to the reference without an axial wall (ja) or radial deflectors (jr). It is clear that a 7mm axial clear-

ance only slightly reduces losses, whereas 4 and 1mm clearances significantly improve them. Radial clearance only slightly affects the losses, as previously mentioned.

1.3.5 Key takeaways

From these studies, some key takeaways should be considered for further work with this thesis:

- Avoid/reduce bubble formation.
- The bubbles in the oil act as a non-lubricating component.
- General agreement that altering the geometry of the transmission housing is a reasonable area of investigation.
- Redirecting the oil flow for an optimal flow pattern is something that should be investigated.
- Reduced axial clearence seem to improve churning losses significantly.

1.4 Aim

The goal of this project is to fill the knowledge gap that exists regarding churning losses and create a guide that helps with further gearbox housing designs. The plan is to develop at least 3 different housing insertions with different wall distances to the gears. The aim is to explain how different insertion geometries affect the churning losses when varied.

An underlying issue with closing the distance to the gear wheels is that it might lead to cooling problems, leading to further losses. This is an additional goal for the project to investigate if time allows (more on limitations under Demarcations). The baseline of the test rig is a pair of gearwheels in a rectangular box filled with oil. This will serve as a reference for all measurements and the ambition is to add geometry in this box that alters the housing/wall distance to the gear wheels.

Important to note is that the main high-level objective from this study is to give design guidelines that can increase the efficiency of Volvo's transmissions by reducing churning losses.

1.5 Demarcations

To create a project that is suitable to complete within the time window, there will be some demarcations made with regard to the available resources, time and overall knowledge in the subject. One master student will complete the project in a time

span of about 20 weeks and the work can therefore not be divided (resource- and time-limited). The work will not handle a complete transmission, instead it will only be looking at a single gear-pair in a test rig. This is to isolate the churning losses from other transmission losses. However, it is important to note that there could still be other losses in the test rig system and run-to-run variance that affect the results. This directly impacts the accuracy of the testing and is a limitation of the project. The testing will also only be looking at a set oil-level height and temperature, to limit the number of possible test configurations. When it comes to the transmission housing itself, this will be kept constant based on the Volvo AMT/I-shift gearbox [Volvo Trucks, 2026]. Instead, the work will focus mainly on studying how insertions inside this housing will affect churning losses.

The work consists of three main parts: prototyping (CAD, 3D-printing), simulation and testing. The total time scope limits the extent of each part and more time will be spent on testing and prototyping. The simulation part will therefore be mainly limited by time. The prototyping, as mentioned before, will be conducted using CAD software (Catia V5) and 3D printing. The material properties of real transmission housings will not be represented; only the geometrical shape will. There could also be other differences in the prototypes that differ them from their real implemented counterpart (size, thickness etc). This, in turn, along with finite simulation time, limits the work in thermal tests/simulations and how wall geometry affects the cooling performance of the gears. However, this should have a limited effect on the churning losses during test-rig runs/simulations.

The project at large will not have a specified budget, instead Volvo Group will provide the necessary means and materials to complete the work as long as it is reasonable and defensible. The goal is to ensure a reliable source on how housing geometry affects churning losses.

1.6 Social, ethical and ecological aspects

The increasing need for transport with the help of heavy-duty vehicles has led to an increase of CO_2 emissions. As a result of this, the EU implemented emission regulations in 2019 for these types of vehicles. Regulations that aim to decrease the CO_2 emissions by 45 % in 2030 compared to 2019 [European Commission, 2023]. Manufacturers are expected to meet these regulations. Volvo Group is one of them and needs to innovate reach the EU's goals as well as their own climate ambitions. Volvo Group has set a goal of -50 % absolute emissions of their total operation compared to 2019. For trucks, this goal is set to -40 % emissions per vehicle kilometer [Volvo Group, 2026]. There are many factors that contribute to these emission reductions and Volvo Group is actively working on many levels to reach its goal. Transmission development is therefore one key aspect that can aid that ambition.

As mentioned under section 1.1, 5.1 % of energy used by heavy-duty vehicles is consumed by losses in the transmission. Churning losses are a part of that and occur due to the splashing of transmission oil inside the transmission housing. The

oil is necessary to ensure proper lubrication and cooling for the gears. The absence of oil would dramatically decrease the transmission lifespan and catastrophic transmission failures would be much more prevalent. Reducing these losses while maintaining a reliable operating conditions is therefore of importance.

Electric trucks/vehicles also use different geared transmissions in many cases and they are becoming increasingly popular. The efficiency of electric drivetrains is very high and the motor efficiency alone can reach well above 90% in many scenarios. This trades blows with transmission efficiency, meaning that improving the transmission efficiency is potentially as important as improving motor efficiency. An improved transmission, along with other improvements in the drivetrain, will lead to increased range, less emissions per driven kilometer (ICE), longer transmission lifespan and a good step towards the heavy-duty climate goals for 2030.

2

Theory

This chapter presents the theoretical foundation needed to understand the thesis. It goes through the basics of transmission operation and presents a quick overview of the Volvo AMT gearbox and its features. Transmission losses and their causing mechanisms are explained along with the aeration of oil. This is followed by an explanation of measurement uncertainties and what tools can be used to quantify them. Lastly, SPH is explained in more detail.

2.1 Basic transmission operation

The figure below (Figure 2.1) shows a simple 5-speed transmission sketch with most fundamental parts listed. It consists of three shafts: input (From engine), layshaft, output (To differential), gears, synchronizers (purple in the figure), bearings and a selector fork with a gear lever.

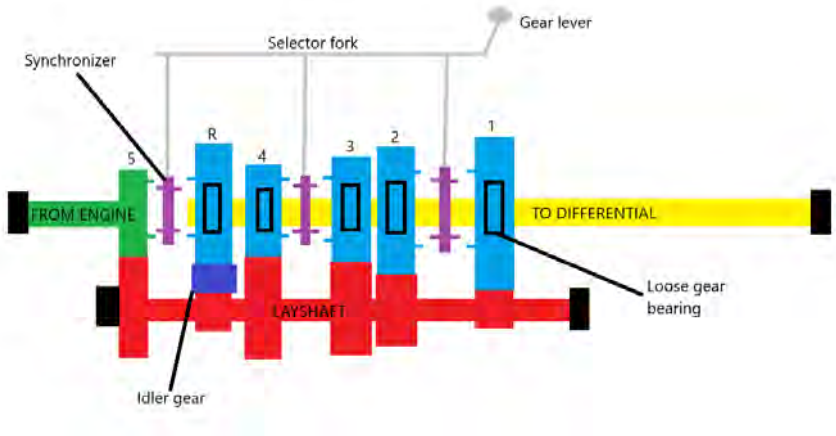


Figure 2.1: Basic 5-speed manual transmission sketch

The bearings are mounted at the end of each shaft, where they would be mounted on the transmission housing. There are also bearings inside the loose gears (blue in the figure) for them to spin freely when not engaged. The layshaft has fixed gears on it that spin with the shaft and these in turn, spin the loose gears. The synchronizers are moved by the selector fork, which is moved by the gear lever inside the vehicle. For example, when first gear is engaged, the synchronizer is moved forward and locks the

loose gear to the output shaft. This means that the power is now being transferred through the first gear. Finally, the idler gear, located between the layshaft and the reverse gear. This just reverses the direction in which the reverse gear will spin, meaning that the vehicle can reverse. To calculate a ratio between two gears the following formula is used:

$$Gear\ ratio = \frac{Z_U}{Z_L} \tag{2.1}$$

Where Z_U is the number of teeth o the upper gear (35 in this thesis) and Z_L is the teeth on the lower gear (39 in this thesis), yielding a gear ratio of 0.897 in that case. Accordingly, an upper gear speed of 1200 RPM would mean that the lower gear spins at about 1077 RPM [CarTechBooks, 2015].

The Volvo AMT gearbox (Figure 2.2) is a development of the basic manual transmission but instead of moving the synchronizers manually via the selector fork, it is done automatically (hence AMT).

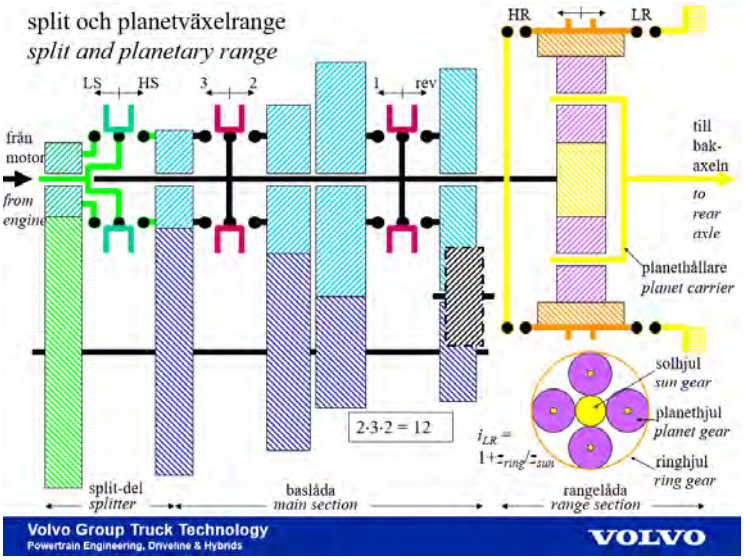


Figure 2.2: Diagram of a Volvo AMT, courtesy of TTI

This transmission introduces 2 new concepts, the splitter and range section. The splitter allows the vehicle to have a low-speed ratio (LS) and a high-speed ratio (HS) for different use cases. LS can be used for better startability of the vehicle, while HS is mostly used during cruising speeds. The range section consists of a planetary gear-set and is there to increase the possible range of gear ratios even further [Volvo Trucks, 2022].

2.2 Load independent losses

As mentioned in section 1.1, the main focus of this study is load independent losses and is what this section will focus on. These can also be referred as no-load losses and vary with the speed of the transmission.

Investigations have shown that load independent losses (P_{LGO}) are responsible for a substantial part of power losses (depending on driving conditions). Therefore, they play a big role in the development of a transmission. These losses can be categorized based on their cause of formation; churning, squeezing and windage [Liu et al., 2018]:

$$P_{LGO} = P_{LGO,C} + P_{LGO,S} + P_{LGO,W} \tag{2.2}$$

The dip lubrication mechanism in the transmission and circulation of the gears, is the cause of churning losses ($P_{LGO,C}$). The oil provides lubrication/cooling as mentioned but requires work to move through, leading to losses. Squeezing losses ($P_{LGO,S}$) stem from oil being squeezed out from tooth crevices in the meshing. This causes the oil to be displaced in the rolling and axial directions of the gears. In the rolling direction, the oil film is displaced on the tooth flank, while the axial direction displaces oil by squeezing excessive liquid out of the tooth gap. This process requires work, leading to losses but is necessary for gear cooling [Liu et al., 2018].

Windage losses ($P_{LGO,W}$) originates from the secondary medium which is air in most cases. It follows the same principle as churning, as air creates resistance when the gears are through it but at a much smaller degree. This is due to air having a lower density compared to oil [Liu et al., 2018]. The load independent losses are illustrated in the figure above (Figure 2.3). It is an effective way of visualizing how the losses occur.

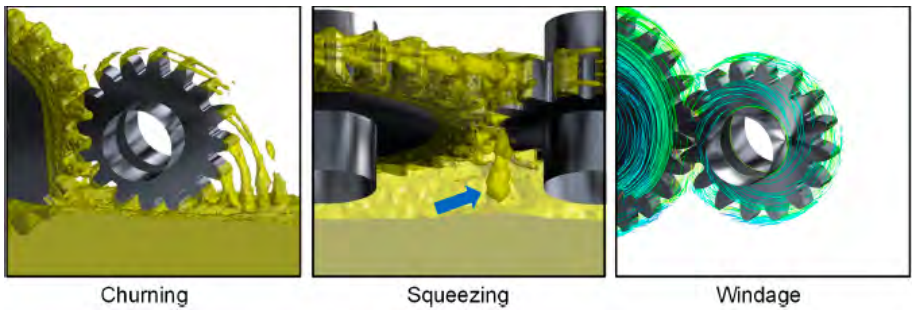


Figure 2.3: Illustration of load independent losses based on a CFD simulation, courtesy of [Liu et al., 2018]

2.3 Oil aeration

The presence of air in the oil is called aeration. This happens either when the gears are rotating and mix air with the oil, or during splashing of the oil onto the free surface. This can vastly change the fluid properties, both density and viscosity. The rate of bubble generation/aeration is proportional to the rotational speed of the gears. The higher the speed the higher the rate of aeration. It is impossible to avoid aeration as the gear teeth create low-pressure regions between them. This region subsequently traps air inside the oil, resulting in an air bubble. The bubbles in oil act

as insulators, reducing the conductivity and resulting in higher gear temperatures. This will lead to higher losses in the transmission. [Hartono, 2014].

2.4 Measurement uncertainties

When measuring anything with instruments or sensors, there will always be some uncertainties/inaccuracies to take into account. Uncertainties that can stem from instrument limitations or simply user error. To ensure that these uncertainties are considered, there are some methods that can be used. Firstly, it is important to take more than one measurement for a single case, to get a mean value for that specific case. The average/mean can be calculated using the following formula [Deardorff, UNC]:

$$\bar{x} = \frac{x_1 + x_2 + x_3 + ... + x_i}{N} \tag{2.3}$$

Where x_n is the measurement taken and N is the total number of measurements. Deviations will also arise from different measurements and is important to consider. As previously mentioned, instruments have inaccuracies and the measurements should be within the specified inaccuracy to be considered valid. Standard deviation (s) is a common way to consider these measurement deviations and the formula below is used [Deardorff, UNC]:

$$s = \sqrt{\frac{1}{N-1}\sum_{i=1}^{N}(x_i - \bar{x})^2} \tag{2.4}$$

There will, of course, be additional uncertainties that are difficult to account for, especially in the transmission test rig to be used later. Uncertainties that, for example, could arise from losses that are separate from the load independent losses. Therefore, it is important to take multiple measurements and account for these deviations.

2.5 Smooth Particle Hydrodynamics

SPH is a meshless particle-based method that has seen increasing usage in transmission design. The foundation of SPH is the use of Lagrangian transportation of information between particles. This is the mesheless nature of the method. Instead of passing information/mass through a mesh (Eulerian transportation), like traditional CFD, each particle carries its own information/mass. This makes the method inherently mass conservative, seeing as there is no mass transport between particles. In this model, the acceleration of an individual particle is obtained from: external forces (gravity or surface tension, etc.), fluid viscosity (friction between particles), and the local pressure gradient [DiveCAE, 2020].

The kernel smoothing, used by this method, is used to handle different physical quantities. This essentially simulates the multiphase flow of air and oil that exists inside a gearbox and captures the complex dynamics of liquid-air interference

[Shao et al., 2026]. As the name suggests, SPH simulations work by simulating liquids as particles that can move around. Figure 2.4 shows a 2D example of how particles in an SPH simulation can move around. The particles can interact with each other and this effectively simulates multiphase flows. This can, of course, be done in 3D as well [DiveCAE, 2020].

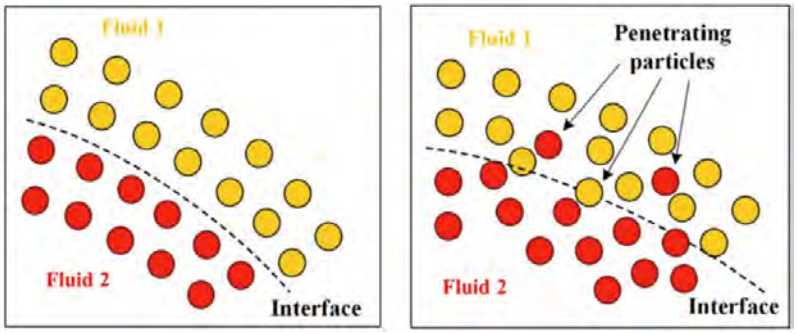


Figure 2.4: 2D example of how SPH particles can move, courtesy of [Dong et al., 2022]

The kernel smoothing previously mentioned uses continuous interpolation. This works by having a point of interest and taking neighboring points of information in to account. Each point has a weight assigned to it. Closer points have higher weights, while farther ones have less weight.



Figure 2.5: Two examples of kernel functions, courtesy of [DiveCAE, 2020]

This creates a Gaussian bell-shaped curve (see Figure 2.5). As the radius of the kernel function becomes smaller, the more precise the approximation of the fluid becomes. However, SPH is not continuous, and discretizations are required to obtain information on the fluid flow in regions where there are no particles available. This is done through the following steps [DiveCAE, 2020]:

- Determine the neighboring particles inside the kernel radius.
- Compute the kernel weight at the centers of the neighboring particles.
- Weight the physical quantity carried by the neighboring particles (the curve height) by the kernel values.

- Sum the values thus obtained.

3
Methods

To begin, the work involves a literature study on churning losses to understand their mechanics and causes. This serves as a good foundation and starting point for the project, which helps to explain different discoveries later. Another purpose of the study is to aid the prototype design process. Understanding the mechanics of losses will lead to more informed design work. Simulations also benefit from such a study, as more educated discussions and conclusions can be made after studying the results. Results can be discussed and deemed reasonable/unreasonable on the spot, something that would take longer without a robust theoretical foundation. There is also a part focusing on previous similar studies, where key takeaways are taken into account for further evaluation or consideration. However, the theory is only the beginning of the project. The main part of the work will be divided in to three bigger parts:

- CAD using Catia V5 for modeling and prototyping
- Simulating using SPH
- Testing different insertion configurations using the test rig

3.1 CAD and prototyping

The first major part is the CAD and prototyping phase. This will use lessons learned from the literature study and apply them to virtual models. This part will lay the foundation for the simulations and eventually for the testing as well. The task here is to establish a framework of how the geometries should be designed and key focused design areas based on the study of similar reports. The work will start with rough sketches to get an idea of the general design of the insertions. These rough designs will later be refined to achieve a desired look and predicted functionality. An available CAD model of the test rig will be used and this is where the insertions will be placed into. The insertion models will be parameterized to allow quick geometry changes and iterative design changes during the project. The test rig model and the insertions will create assembly models that will be used in the next step.

3.2 SPH simulation

The simulation part of the project will use an SPH solver in STARCCM+. This type of solver suits simulations of gear wheel interactions better than traditional CFD due to the meshless nature of the method. This saves time by not having to recalculate meshes for rotating parts. The simulations will use the previously mentioned assembly models as a base. This will virtually serve as the test rig setup. The first task is to simulate a baseline result, meaning no usage of insertions to get a reference to compare against. This will be done multiple times for different predetermined rotational speeds and a set oil level and temperature (see section 5.2). When the baseline results have been gathered, a complete assembly model (including insertion) will be simulated under the same conditions. These results will then be directly comparable to the baseline and potential improvements might be visible. The findings here will be forwarded and taken into account when using the test rig later.

3.3 Test rig testing

The last major part of the project is the testing using the test rig. This will be the most extensive and time-consuming part of this work. Here, the CAD models of the insertions will be 3D-printed for testing. These insertions will be placed into the test rig, similarly to the previous assembly models, and tested using a sweep of rotational speeds, a set oil level, and temperature. This will make some results directly comparable to simulations, and conclusions about simulation validity and results can be drawn. Furthermore, in the tests, a different oil than the real transmission oil will be used to eliminate the need for a heating loop. At room temperature, this oil replicates the operating conditions of transmission oil at elevated temperatures (about 65°C to 70°C). More refinements and design changes are likely to be made in this step, due to how the project evolves and findings made under testing. This means that there will most likely be more insertion configurations tested that cannot be directly compared to any simulation.

Finally, after finishing the testing part, it is time to evaluate the extensive testing/simulations of the different insertion designs used. Different versions will be presented and compared, along with their pros and cons. The goal here is to have at least three different designs with different wall distances to the gear wheels. Based on the results, recommendations will be made and what further studies should focus on, if one chooses to continue in these tracks.

4

CAD and prototyping

This chapter describes the development of insertion concepts, their CAD implementation, and the practical mounting solution used for testing churning losses. It also describes the modifications made to the CAD models before 3D printing and the selection of concepts that are taken into the simulation step of the thesis.

4.1 Design process

The design process starts by evaluating concepts through a matrix and eliminating unwanted ones. The concepts that are taken into further consideration are then made into simple sketches. Based on these, the CAD models can be created along with their mounting features.

4.1.1 Concept matrix

To limit the number of concepts with the time scope of this project in consideration. A concept matrix (Table 4.1) is created. This matrix limits the axial and radial distances to three in each direction and the coverage of the proposed walls to Full/Half coverage. The distances refer to the distance between the gear wheel and wall (axially and radially). Full coverage is defined by covering the full diameter in width of the lower gear wheel. Half coverage is conveniently half of this, meaning that it covers only the width of the radius on the right side of the lower gear wheel. All geometries reach a maximum height of the radius of the lower gear wheel, i.e the middle. "No wall" indicates no added geometry inside the transmission housing, meaning that it is the reference for all measurements.

Table 4.1: Concept Matrix

		Axial Distance						
			5mm		1mm		4mm	
Radial Distance	**Width**	No wall	Half	Full	Half	Full	Half	Full
	No wall	**Ref.**	–	–	–	–	–	–
5mm	Half	–	–	–	–	–	–	–
	Full	–	–	–	–	–	–	–
10mm	Half	–	–	–	–	–	–	–
	Full	–	–	–	–	–	–	–
15mm	Half	–	–	–	–	–	–	–
	Full	–	–	–	–	–	–	–

There are a total of 49 possible concepts in the table above, including the reference. Some of which are not possible to realize. In Table 4.2, many of the concepts have been eliminated for different reasons and those considered are marked with X. First of all, concepts marked with NA are concepts that would not work in real life. These fully isolate the lower gear wheel from the surrounding oil, meaning that no lubrication or cooling is provided. Furthermore, based on the findings in the study under subsection 1.3.4, only one axial and two radial distances (5mm axially, 5mm and 10mm radially) are considered. The axial distance should be small to minimize losses, while the radial distance has a less significant effect. Another requirement is that the concept should provide oil flow guidance in the radial direction based on the findings under subsection 1.3.1 where it was stated that wall profiles should be investigated to guide the oil flow.

Table 4.2: Concept Matrix with selected concepts

		Axial Distance						
			5mm		1mm		4mm	
Radial Distance	**Width**	No wall	Half	Full	Half	Full	Half	Full
	No wall	**Ref.**	–	–	–	–	–	–
5mm	Half	X	X	X	–	–	–	–
	Full	X	X	NA	–	NA	–	NA
10mm	Half	X	–	–	–	–	–	–
	Full	–	–	NA	–	NA	–	NA
15mm	Half	–	–	–	–	–	–	–
	Full	–	–	NA	–	NA	–	NA

This leaves a total of 6 concepts, plus the reference for further consideration in the thesis. The concepts aim to reduce churning losses by reducing axial clearance, while providing a more favorable flow pattern than the one found in Figure 1.2. The hope is also that these geometries will provide less aerated oil in the system, further

improving cooling and lubrication performance. The concepts that utilize "No wall" axially aim to investigate how the radial geometry affects the losses without any axial interference.

4.1.2 Sketching

From Table 4.2, there are only three different concepts that differ by three different radial distances (9 concepts total). To get a rough starting point before doing any CAD, simple sketches are made and can be seen in Figure 4.1. All of these are subject to change as the project evolves. The black square represents the transmission housing, along with the upper and lower gears. The red parts of the sketches represent radial geometry and the blue parts are axial walls/geometry. The rotating direction of the upper gear wheel is clockwise while the lower spins counter-clockwise.

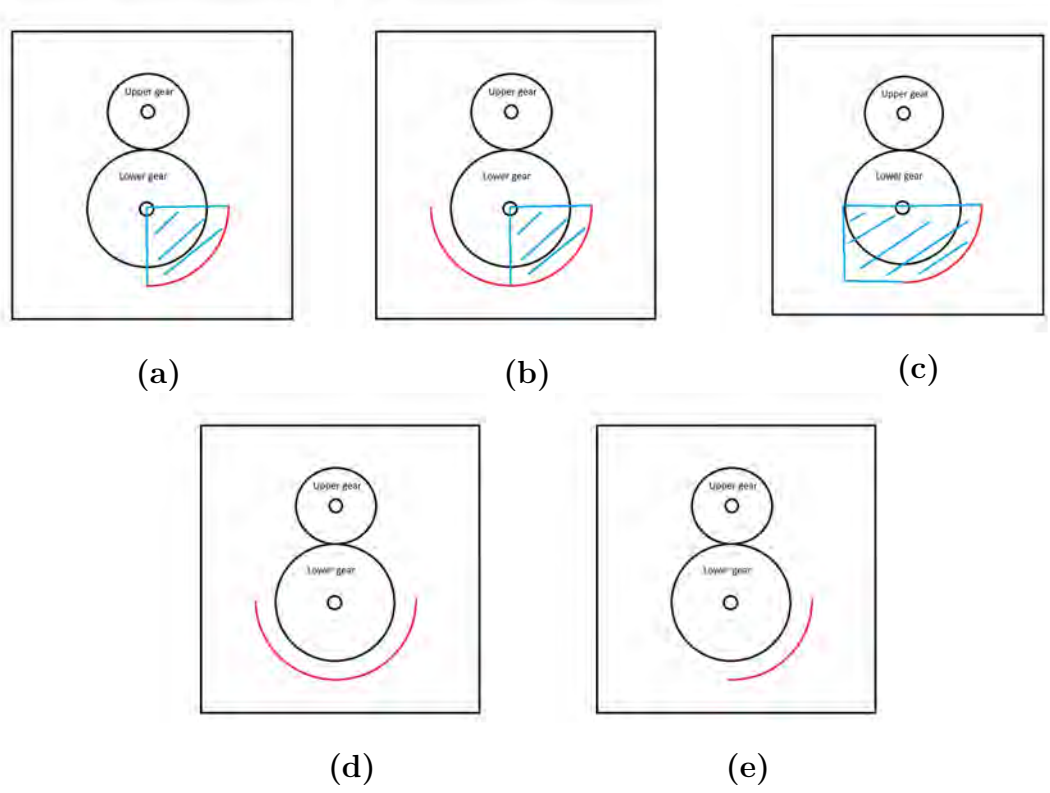


Figure 4.1: Sketches of the investigated configurations: (a) Half axial + Half radial, (b) Half axial + Full radial, (c) Full axial + Half radial, (d) No axial + Full radial, (e) No axial + Half radial.

The different configurations shown in Figure 4.1 can be described as follows:

- **Figure 4.1a – Half axial + Half radial:** Geometry is only added to cover the bottom half of the lower gear, and the oil is free to enter it radially.

- **Figure 4.1b – Half axial + Full radial:** Extends the radial geometry of the previous sketch to cover the entire bottom half of the lower gear. Here, the oil is free to enter axially where no axial wall is present.

- **Figure 4.1c – Full axial + Half radial:** Removes the full radial coverage and instead adds a full axial coverage that spans the whole bottom half of the lower gear. In this configuration, the oil enters radially.

- **Figure 4.1d – No axial + Full radial:** Utilizes only a radial wall that spans the entire diameter of the lower gear wheel. This concept is completely open in the axial directions, making the oil enter from these directions.

- **Figure 4.1e – No axial + Half radial:** Removes half of the radial wall from the previous sketch. Here, the oil is free to enter axially at all times and radially where no radial wall is present.

4.1.3 Half axial + Half radial

The first design is from Figure 4.1a, combining a Half axial and Half radial concept (Figure 4.2). The color coding is the same as before. The blue geometries are axial walls, while the red geometries are radial. There is an additional cutout on the axial walls to accommodate fo the gear hub of the lower gear wheel (see Figure 4.8). This width would interfere with the axial wall at low axial distances. Note that the axial walls have a slight draft angle of 2 degrees outward to simulate a casted part. This is used for all insertion geometries that utilize axial walls.

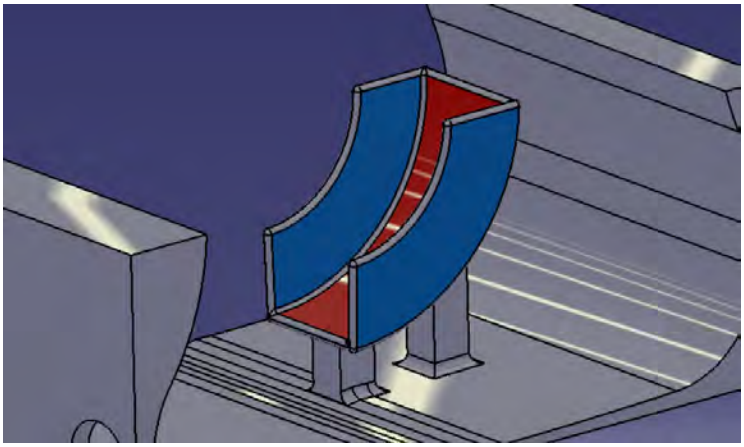


Figure 4.2: Half axial + Half radial in CAD

This design provides the lower gear wheel with unaffected oil, upstream of the rotating direction (left side in the figure). The axial walls cover the bottom quarter of the gearwheel, while the radial geometry changes the direction of oil splash. Both of these might force the oil to move radially through the geometry downstream (right in the figure).

4.1.4 Half axial + Full radial

The Half axial with Full radial design (Figure 4.3) extends the radial geometry of Figure 4.2. The same principles apply downstream of the gearwheel, but upstream

of it is different.

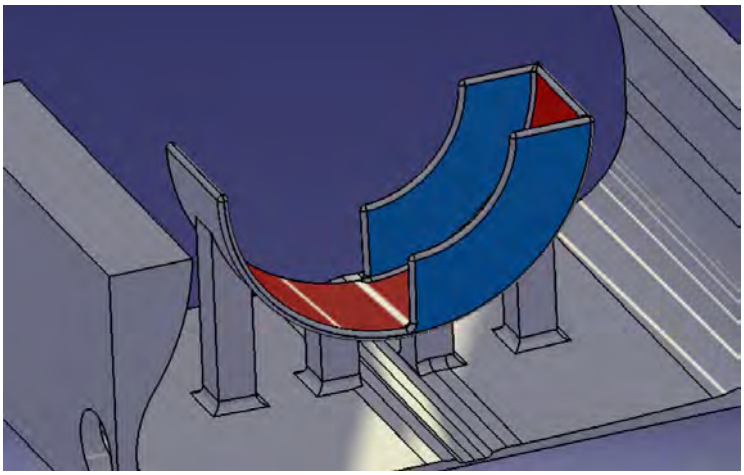


Figure 4.3: Half axial + Full radial in CAD

The oil upstream of the gearwheel is now affected by radial geometry, which might further guide the oil radially before the axial walls by acting as a ramp. This geometry might also catch some of the oil that splashes over both the lower and upper gearwheels. Two additional legs are introduced on the extended radial part to support the elongated geometry.

4.1.5 Full axial + Half radial

The design in Figure 4.4 combines a Full axial with Half radial walls, which is an extension of the axial walls from Figure 4.2. The downstream oil is affected by the same type of geometry, but the upstream oil is once again affected by a different geometry.

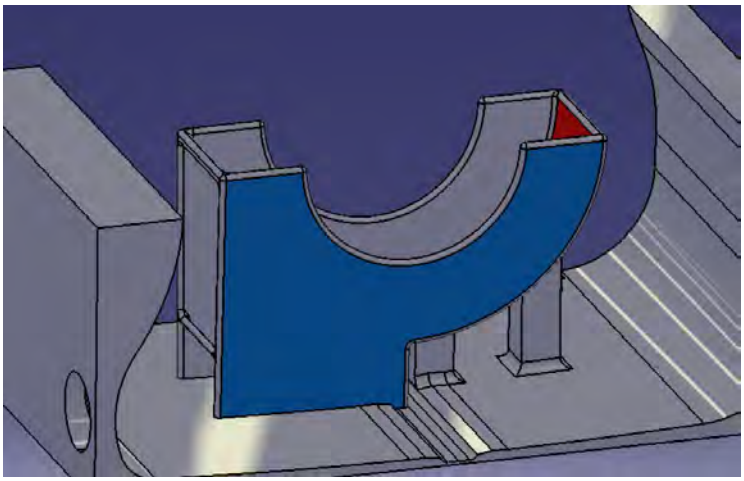


Figure 4.4: Full axial + Half radial in CAD

The axial walls fully cover the bottom half of the lower gear wheel and might affect the oil that enters to that gear. The full coverage of the axial walls might also

prevent oil from exiting the geometry axially until it leaves the area of effect. There are two horizontal support elements on the left side of the axial walls to prevent them from flexing inward/qoutward, in combination with the axial walls extending to the bottom of the transmission housing for further stability.

4.1.6 No axial + Full radial

The design in Figure 4.5 completely removes the axial walls and utilizes a full radial coverage. This design is the same as in Figure 4.3 but without the axial walls. Both downstream and upstream oil can now be affected by a radial plate without any axial interference.

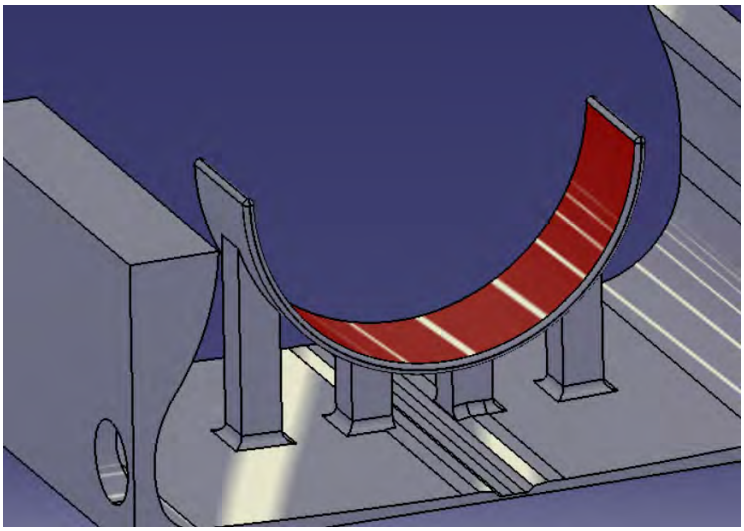


Figure 4.5: No axial + Full radial in CAD

The full coverage of the radial plate might guide the oil further upwards, but nothing prevents the oil from escaping axially. Oil splashing over both gear wheels might be caught by the radial plate, as mentioned previously. The same 4 supporting legs are present in this design as well.

4.1.7 No axial + Half radial

The final design (Figure 4.6) removes half of the radial wall from Figure 4.5. The radial geometry might now only affect the oil downstream and leave the upstream oil unaffected. There is still no axial interference.

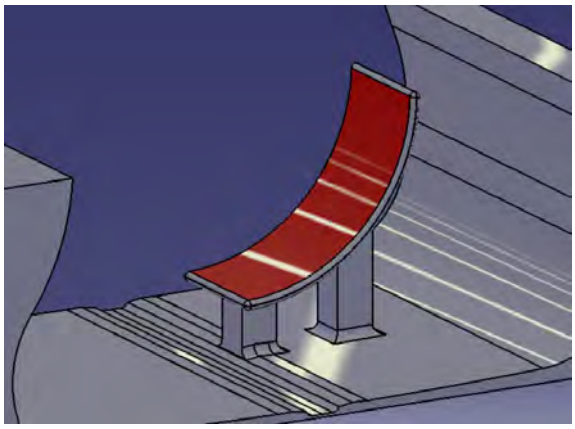


Figure 4.6: No axial + half radial in CAD

The radial plate is thought to guide the oil splash upwards, but nothing prevents it from escaping axially again. The supporting legs of the geometry are the same as those found in Figure 4.2.

4.1.8 Insertion mounting

The insertions need to be mounted securely to the transmission housing. This requires a robust mounting system that allows for quick swapping of insertions while maintaining stability. It should also have a minimal effect on the oil flow inside the transmission housing/test rig, ensuring that the results are primarily due to the inserted geometry. In the test rig, the transmission housing is split into a top part and a bottom part (see Figure 4.7).

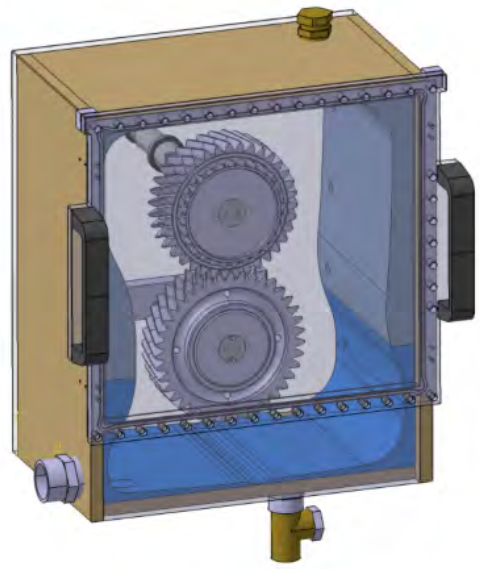


Figure 4.7: 3D-model of test rig box with transmission housing, bottom part in blue and top part in gray, courtesy of [Fransson and Eliasson, 2021]

The first thought was to modify the geometry of the housing to include the inser-

tions as part of it. This would eliminate any need to further secure the inserted geometry. However, from a 3D printing perspective, this is not optimal. The housing part should be printed on its side, resulting in a good finish with limited support elements (additional printing to stabilize a print during 3D printing). Including insertions during the printing phase would require numerous support elements, which could also result in a poorer print finish.

The second approach was to separate the two parts into distinct prints. This would leave the bottom part of the housing largely the same but with a slight modification for mounting the insertions on it. The print quality of the inserted geometry would increase as it is now its own print, resulting in a more precise representation of the digital model. The modular nature of this concept would be more amenable to future insertions, since only the actual inserted geometry needs to be printed for further testing. However, repeated use of the mounting system could wear it out, resulting in potential variations between runs. See Figure A.1 for more details on how it would look.

4.1.8.1 Final mounting concept

The final mounting concept was chosen as a complete print of the lower part of the transmission housing along with the inserted geometry (see Figure 4.8).

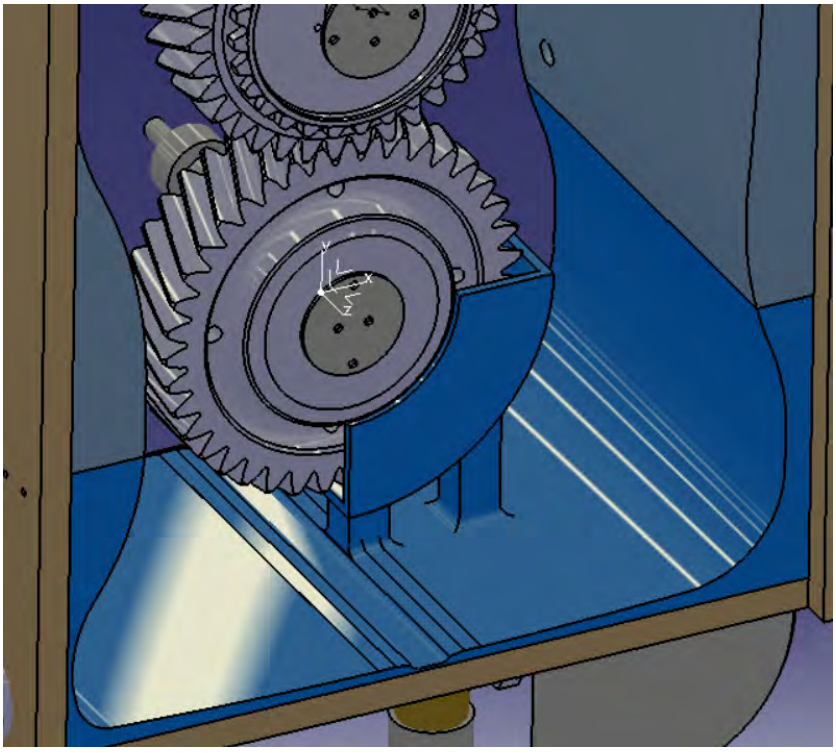


Figure 4.8: Lower transmission housing with insertion, blue in figure

The 3D printers at TTI are of the SLS (Selective Laser Sintering) type. This method prints the part with a high-power laser inside a powder bath, which acts as a constant

support. This effectively eliminates any constraints regarding overhang of geometry, warping walls, etc [Formlabs, 2021]. All the concerns from the first thought above are therefore addressed. This means that the 3D printing can commend with minimal geometrical constraints.

4.1.9 Modifications before 3D printing

The limitation of space inside the test rig poses a few practical challenges to placing geometry inside it. When both gear wheels are installed (see Figure 4.7), it is impossible to place a complete lower part of a transmission housing without interfering with the gear wheels and/or their axles. Removing these would enable the placement of the lower housing, but installing the lower gear would still be impossible when using insertion geometries with axial walls. These prevent the lower gear wheel from mounting axially. This partial disassembly between different insertion geometries also wastes valuable testing time. Figure 4.9 shows the open test rig box with the right side of the lower transmission housing divided into two parts. One containing the insertion geometry and the other being the housing wall.

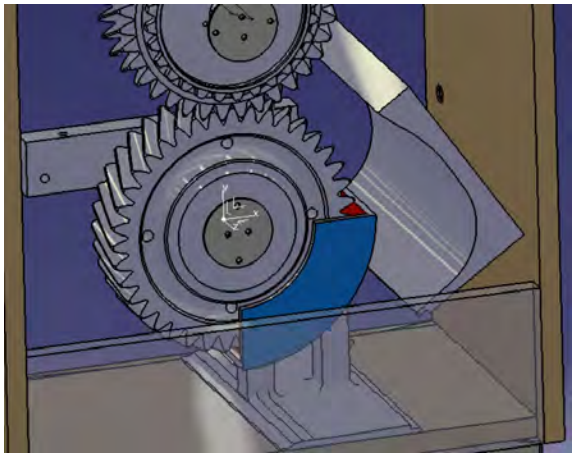


Figure 4.9: Test rig box with lower housing geometry and insertion split

This enables the installation of the lower transmission housing without removing any of the gear wheels or their axles. Note the slight overlap of the parts where they meet at the bottom of the test rig box. This overlap ensures the correct placement of the parts and provides a downward force on the insertion part when the top of the transmission housing is positioned above, further locking it in place. The same principles also apply to the left side of the transmission housing. This means that when the lower transmission housing is placed inside the test rig, it consists of 4 different parts that are interlocked. The nature of this makes the lower housing more modular, as individual parts can be interchanged without removing the complete housing. More details on the specific parts can be seen in Appendix A, Figure A.2.

4.2 Selected designs for SPH

The simulation time is limited in this thesis and therefore, all insertion concepts cannot be simulated. An important factor is to create a baseline of results upon which further conclusions can be drawn based on. The concepts/insertions chosen are listed below:

- Reference (no walls)
- Half axial + Half radial insertion (subsection 4.1.3)
- Full axial + Half radial (subsection 4.1.5)

The reference is a must and creates baseline/reference results to which added insertions can be compared to. Without this, it is difficult to draw any conclusions at all. The selection of the Half axial + Half radial insertion is motivated by the fact that this specific geometry remains unchanged in three of the insertion concepts. Simulating this insertion might yield results that can be linked to these concepts and is, for this reason, an obvious choice. The Full axial + Half radial concept is interesting as it evaluates how a full axial wall affects the results. It is also the only concept that utilizes this geometry and might yield interesting results.

5

SPH simulation

In this chapter, the SPH simulation methodology that will be used to study churning losses is introduced. It goes through the pre-processing steps before a simulation can be started, along with the selected physics models. Finally, it defines the operating conditions for each model to ensure a standardized comparison of the results.

5.1 Pre-processing

This section explains how a sealed bounded box and surface models for the upper and lower gear wheel assemblies are created. This accurately represents the transmission housing and rotating components for the SPH simulation and is consistent with the test rig configuration. It also highlights the physics models used in the simulation.

5.1.1 Bounded box

When simulating with SPH, a clear boundary/box needs to be created to prevent particles from escaping into unwanted areas. Although the SPH method itself is meshless, the boundaries in the simulation still need to be defined and meshed to a desired accuracy. Based on the test rig box assembly seen in Figure 4.7, a bounded box can be created that should be the shape of the transmission housing. This is done through software called ANSA. The assembly model is saved as a "STEP-file", which is a high-accuracy mathematical representation of the 3D model. When the "STEP-file" is loaded into the software, it is stripped of unwanted parts that do not contribute to the desired box. For example, axles, gears, test rig box walls, etc. The next step is to "fuse" the test rig axial walls with the upper and lower transmission housings. This is done to create a topologically closed volume. The model is now completely sealed, with no gaps, as shown in Figure 5.1.

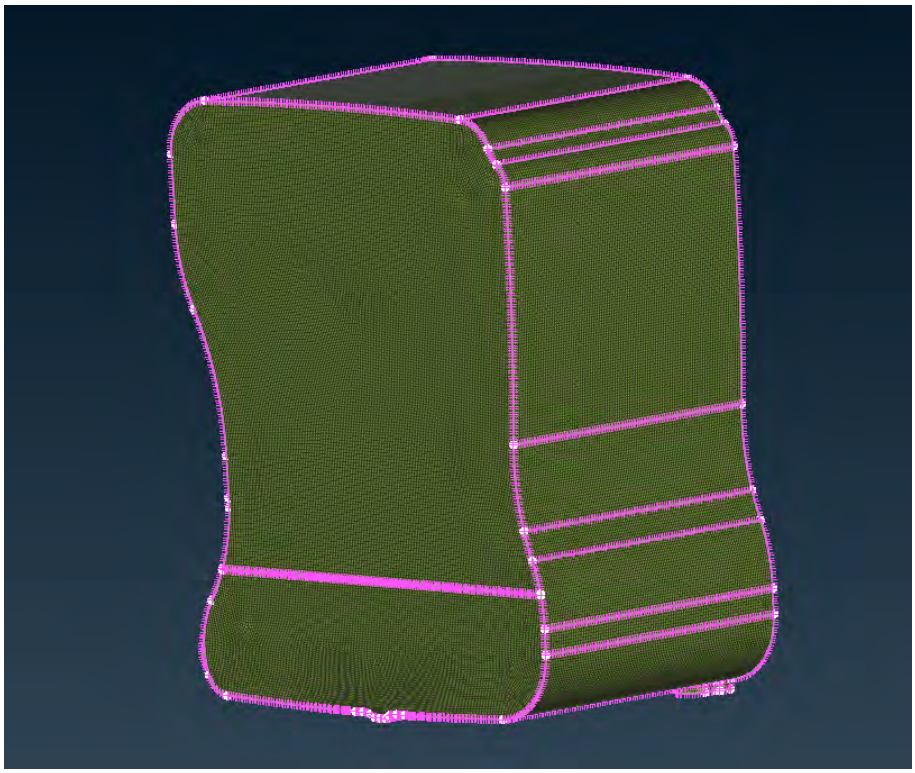


Figure 5.1: Bounded box of transmission housing

Lastly, a mesh is created for the surfaces, which decides the accuracy of the geometry. A finer mesh will better capture the wall geometry and create a more accurate representation of the box, but it will also increase the calculation time. The mesh is generated with a target element length of 1mm and a growth rate of 0.8. This configuration preserves the box's critical geometric features while providing stable boundary conditions for SPH wall interactions.

5.1.1.1 Surface models

With the bounded box in place, the upper and lower gearwheel assemblies can be initialized in ANSA in the same way. The main task here is to identify which parts belong together and rotate at the same speed. The baseline is once again the box assembly shown in Figure 4.7, and the unwanted parts are removed. When this is done, the upper and lower gear wheels, along with their respective parts, are left. These can then be meshed to a desirable accuracy and saved separately (Upper and lower gear wheel assemblies). The insertion concepts follow the same method, removing unwanted parts and meshing the remaining geometry. Figure 5.2 shows the surface models used.

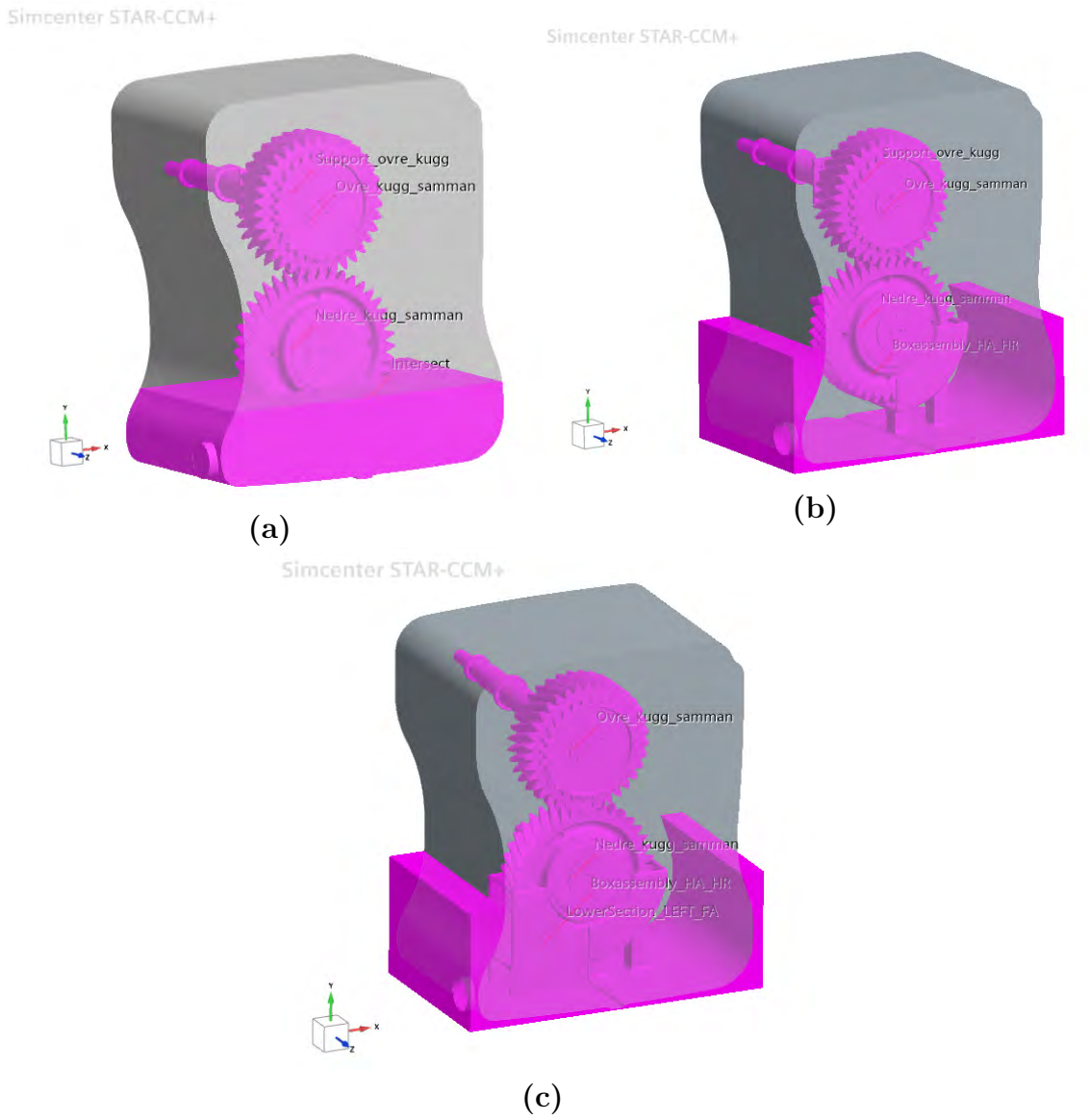


Figure 5.2: Surface models in STARCCM+:
(a) Reference (b) Half Axial + Half Radial (c) Full Axial + Half Radial

In Figure 5.2a, the reference surface model can be seen (no insertion). The bounded box creates the housing shape (gray in the figure) and the remaining parts are inside (purple). Note how the names are separated. "Nedre_kugg_samman" contains everything that rotates with the lower gear wheel and "Ovre_kugg_samman" has everything linked to the rotation of the upper gear wheel. This enables independent control of the gear speeds in the simulation. "Intersect" is the initial oil level in the system. Figure 5.2b and Figure 5.2c show the same model but with an added insertion concept (oil level not visible).

5.1.2 Physics

A complete list of the common and phase-specific physics models are presented in Table 5.1. Gravity is defined as $(0, -9.81, 0)$, acting straight down in the y-direction,

which corresponds to the downward direction in the simulation model.

Table 5.1: Physics Models

(a) Common

Physics Model
Adaptive Time-Step
Gravity
Implicit Unsteady
Incompressible Flow (ISPH)
Laminar
Multiphase
Multiphase Interaction
Smoothed-Particle Hydrodynamics (SPH)
Solution Interpolation
Three Dimensional
Wall Treatment
Particle Remediation

(b) Phase-specific

Oil
Constant density
Laminar
Liquid

The oil is modeled as an incompressible liquid with laminar flow. Using Laminar flow in SPH stems from its Lagrangian transportation, and is used to ensure numerical stability and efficiency. To simulate normal transmission operating conditions, dynamic viscosity (μ) and density (ρ) are set to simulate 97318/97307 oils at 80°C (read more about the oils in subsection 6.1.2). These are kept constant. As shown in the table, only one phase will be present in the simulation (Oil). The two-phase model was unavailable for this thesis, due to licensing, and would likely offer a more accurate simulation of the process.

5.2 Simulation conditions

Each simulation will be completed under the same initial conditions and rotational speed of the lower gear. The oil level is initialized at $92mm$ to replicate the stationary oil level in Volvo's AMT. Two rotational speeds are considered, 1200 RPM and 1800 RPM. The first is used to simulate the trucks' cruising conditions. At these speeds, the upper gear spins at about 1200 RPM. The latter is there to simulate the operation at higher power outputs. The particle diameter is set to $1mm$ as a compromise between calculation time and accuracy. Table 5.2 gives an overview of these conditions.

Table 5.2: Simulation Configuration and Operational Conditions

Parameter	Setting	Description
Rotational Speed (n)	1200 RPM	Upper gear cruising conditions.
	1800 RPM	High-power upper gear operation.
Initial oil level	$92mm$	Height from bottom of box.
Particle size	$1mm$	Diameter of particles in SPH.

Simulating this will yield two different simulation results for each configuration and a total of 4 simulations in this thesis. The first simulations will use the reference design and then the insertion geometry will follow the same procedure. There are no oil inlet/outlet flows simulated, since the task is to represent the test rig where no oil inflow/outflow will be present.

6
Test rig testing

This chapter describes the setup and testing procedure of the transmission test rig used to measure load-independent transmission losses. The rig is configured with a set oil level using an oil that represents the real transmission fluid but at room temperature. There are three main sensors at hand for data gathering; a torque sensor, a speed sensor and a temperature sensor. A test plan is presented that sweeps through a set of RPM points for each insertion configuration in the project. Finally, alternate configurations considered in the testing are introduced.

6.1 Test rig setup

An accurate configuration of the test rig is essential for obtaining reliable and high-quality data. This section describes how the oil level is set, what type of oil is used and the sensors installed for data gathering. It also presents potential accuracies/inaccuracies for each sensor.

6.1.1 Oil level

The oil level is essential for comparisons between different configurations. Variations in oil level can create uncertainties and larger run-to-run variances that affect the comparison between different configurations. It must therefore be kept within an accurate level. Figure 6.1 shows the desired oil level in the system, which is $92mm$ above the bottom of the test rig box.

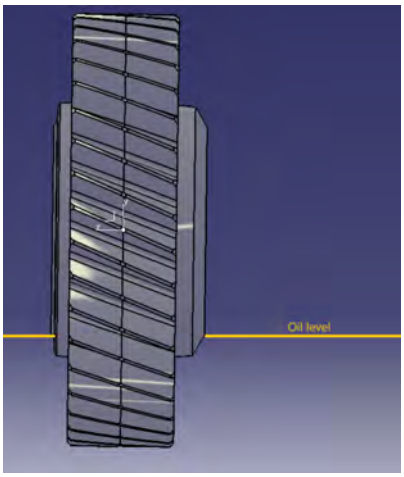


Figure 6.1: Oil level reference for lower gear

Regardless of geometry/insertion inside, the oil level should be kept to match the line in the figure. Henceforth, the volume of oil in the test rig is not of interest, it is the oil level.

6.1.2 Oil type

The oil standard used in Volvo's AMT gearboxes is the 97318/97307 oil specification. It is a fully synthetic transmission fluid designed for long drain intervals. The recommended drain interval is 800 000 km for 97318 and 400 000 km for 97307. They are characterized by their low viscosity, for increased gearbox efficiency, fuel economy and cold weather shifting. The complete specification of the oils is shown in Table 6.1 [Q8Oils, 2026].

Table 6.1: 97318/97307 Oil properties

Property	**Unit**	**Typical**
Density, 15°C	g/ml	0.864
Viscosity Grade	SAE	75W-80
Kinematic Viscosity, 40°C	mm^2/s	61.5
Kinematic Viscosity, 100°C	mm^2/s	10.1
Viscosity Index	-	152
Brookfield Viscosity, -40°C	Pa.s	19.8
Flash Point, COC	°C	240
Pour Point	°C	-57

The ideal oil operating point inside the transmission is around 80°C (Kinematic viscosity $\sim 27.2 mm^2/s$). This would require a heating element/loop inside the test rig. To avoid this, an alternative oil is used that has properties similar to the 97318/97307 oils at 65 to 70°C but at room temperature. This simplifies the testing and speeds up the process by avoiding the waiting time for oil heating. This alternative oil will be called "Oil Type 1" for the rest of the thesis.

6.1.3 Sensors

The test rig utilizes three main sensors: torque, speed and temperature sensors. This subsection specifies each type and briefly describes how they work. It also presents the accuracy of the respective measurements that can affect the reported results.

6.1.3.1 Torque sensor

The torque sensor on the test rig uses a HBM T12HP 100Nm sensor. This sensor measures torque losses within the transmission. Since the project focuses on load-independent transmission losses, this part is the most vital component of the measurement equipment. The sensor has an accuracy of $\pm 0.02 Nm$, giving a very

high confidence in measurement results. All measurements exceeding this accuracy can be viewed as measurable differences.

6.1.3.2 Speed sensor

The speed sensor inside the test rig uses part of the WABCO 4213679222 Transmission repair kit (see Figure 6.2).



Figure 6.2: Speed sensor

This sensor uses internal magnets that induce voltage as a magnetic object approaches and can be utilized as a speed sensor. The sensor measures axially. When a tooth peak approaches, it induces a certain voltage. When there is a tooth valley, the voltage is reduced. This creates a sinusoidal-like voltage pattern with a certain frequency (f) where each peak is a tooth on the gear. Knowing this and the number of teeth on the gear (Z), the rotational speed of the gear (n) can be calculated:

$$n = \frac{f \cdot 60}{Z} \, [RPM] \tag{6.1}$$

The accuracy of the sensors is very high and should provide measurement signals with negligible run-to-run variances.

6.1.3.3 Temperature sensor

The temperature sensor used is a simple Type K thermocouple sensor. This works by measuring a "hot" and a "cold" side. The difference between in combination with the Seebeck coefficient (S), creates a small voltage (V) that corresponds to a certain temperature. Knowing the reference temperature (T_{ref}), it gives a reading of the actual calculated oil temperature (T_{hot}) using the following steps [Analog Devices, 2021]:

$$V = S \left(T_{\text{hot}} - T_{\text{ref}} \right) \tag{6.2}$$

$$T_{\text{hot}} - T_{\text{ref}} = \frac{V}{S} \tag{6.3}$$

$$T_{\text{hot}} = T_{\text{ref}} + \frac{V}{S} \tag{6.4}$$

The typical accuracy of a Type K thermocouple sensor lies within ±2.2°C or ±0.75% (whichever is higher at the given temperature). This will yield small measurement deviations in temperature, as the tests are conducted with oil at room temperature. However, it should not cause problems for this application, since the sensor's main task is to verify that the oil is around the correct temperature and no active temperature regulation is used.

6.2 Testing plan

The experimental test plan used for the test rig in this thesis can be seen in Table 6.2. Each run consists of an RPM sweep that either increases from 600 RPM or decreases from 2100 RPM in 300 RPM increments, with its corresponding oil variant. Note that the RPM listed is for the upper gear wheel. Data recording is done under stable conditions, when the sensor values have stabilized. This eliminates transient behavior in the data and simplifies post-processing.

Table 6.2: Experimental Test Plan: RPM Sweep

Run	Oil Variant	Direction	RPM Points (300 interval)
1	Oil Type 1	Upward ↑	600, 900, 1200, 1500, 1800, 2100
2	Oil Type 1	Downward ↓	2100, 1800, 1500, 1200, 900, 600

The reference is the first configuration that is tested. Each run is completed 4 times, yielding 8 measurements for every RPM point. The remaining configurations, with their respective insertions, then follow the same procedure. When all tests are completed, the reference is run again and compared with the initial test. This is to ensure that the test rig has not degraded between all runs. An overview of the full testing schematic is shown in Appendix B, Figure B.7.

7

Results

This chapter presents the major results found in this project. It includes results from four simulations and testing of all insertion concepts. Lastly, a comparison between simulation and experimental data is presented to link the simulations with the tests.

7.1 SPH simulation

In this section, the results of the different simulation setups described under section 5.2 are presented. The results are shown in terms of power averaged over a certain time. In total, 6 simulations were run on TTI's CPU (Central Processing Unit) cluster using 2304 cores. Each simulation was run until a physical time of three seconds elapsed.

7.1.1 Simulation plots

Below (Figure 7.1) is a figure showing the total power of the reference simulation at 1200RPM (between ~ 0.5 and ~ 2.5 seconds). Note the "spikey" behavior. This is an artifact caused by the SPH particles that move around in the system. Particles might hit or squeeze between gears, causing these high-frequency power surges in the plots. While these instantaneous peaks reach magnitudes of over 1, they are not indicative of the net power loss due to their transient nature and rapid oscillation. The spikes mostly cancel each other out, as they happen simultaneously on the upper and lower gear in opposite directions.

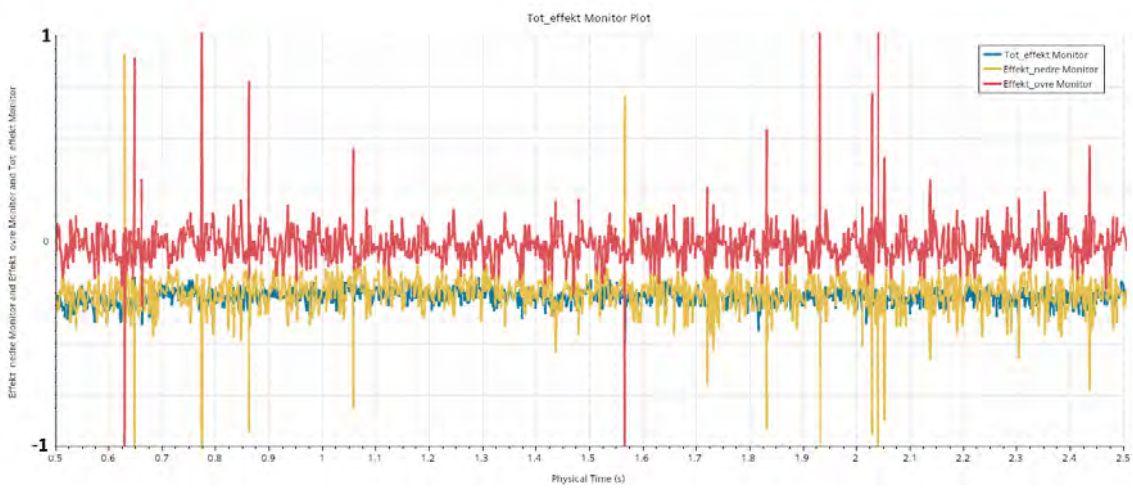


Figure 7.1: Reference total power at 1200RPM

The almost instantaneous return of each spike indicates that the simulation is highly sensitive to the particle size ($1mm$) and that it successfully captures the macro behavior of the system. This fast decay time likely shows that the gears experience positive and negative moments from oil particles splashing/squeezing on them.

7.1.2 Relative performance comparison

To visualize the differences between the configurations, a relative power (P/P_{REF}) bar diagram is created (Figure 7.2). It shows the relative power for the upper and lower gears, as well as the total relative power. The reference is represented by blue bars and the remaining bars are comparisons to their respective reference. All data is gathered between 0.5 and 2.5 seconds, as this is a steady-state operation.

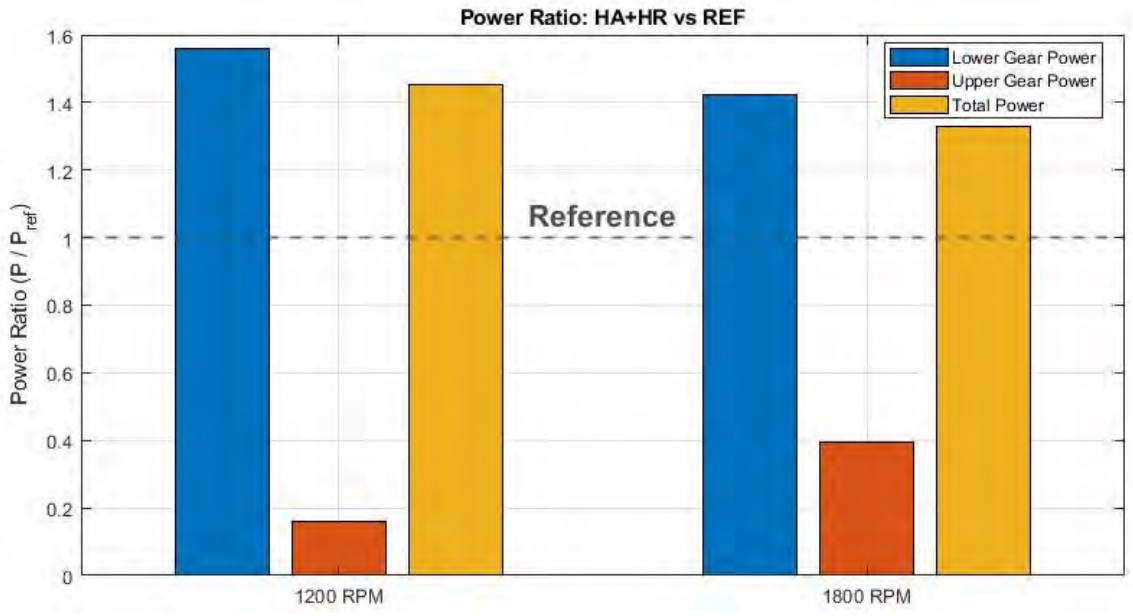


Figure 7.2: Relative power simulation comparison, HA+HR vs REF

The figure above shows that at 1200 RPM, the upper gear power losses exceed the reference significantly by producing about 155% power. On the contrary, the lower gear power is only a fraction of the reference at below 20 %. The total power still exceeds that of the reference, as most of the losses occur in the lower oil-submerged gear. This trend continues at 1800 RPM, but with slightly lower relative total and lower gear power. However, the upper gear's relative power doubled. Figure 7.3 shows the relative power comparison between the FA+HR configuration and the reference.

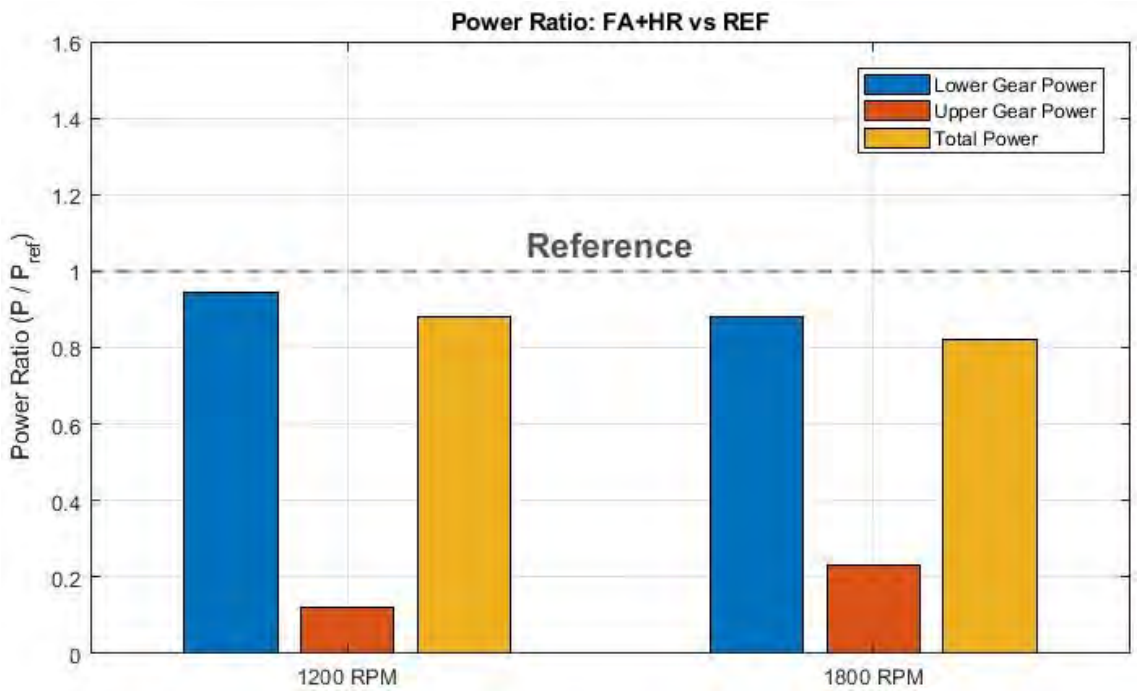


Figure 7.3: Relative power simulation comparison, FA+HR vs REF

The addition of the full axial wall shifts the results significantly. The lower and total relative power are now lower than the reference at both 1200 and 1800 RPM. The same trend with a reduction of relative power between the RPM points is still present, while the upper gear's relative power increases. The biggest reduction compared to the reference is total power at 1800 RPM. This shows a reduction of almost 20%.

7.1.3 Oil flow

To visualize the oil flow pattern in the simulations, velocity magnitude scenes are created. These show the velocity of particles in the system with a range of $0m/s$ to $2.5m/s$. The figures represent the last iteration of the simulations at a physical time of $3s$. Figure 7.4 shows the oil flow of the reference at 1200 RPM from different perspectives. The front cross-section is an axial plane in the middle of the gears.

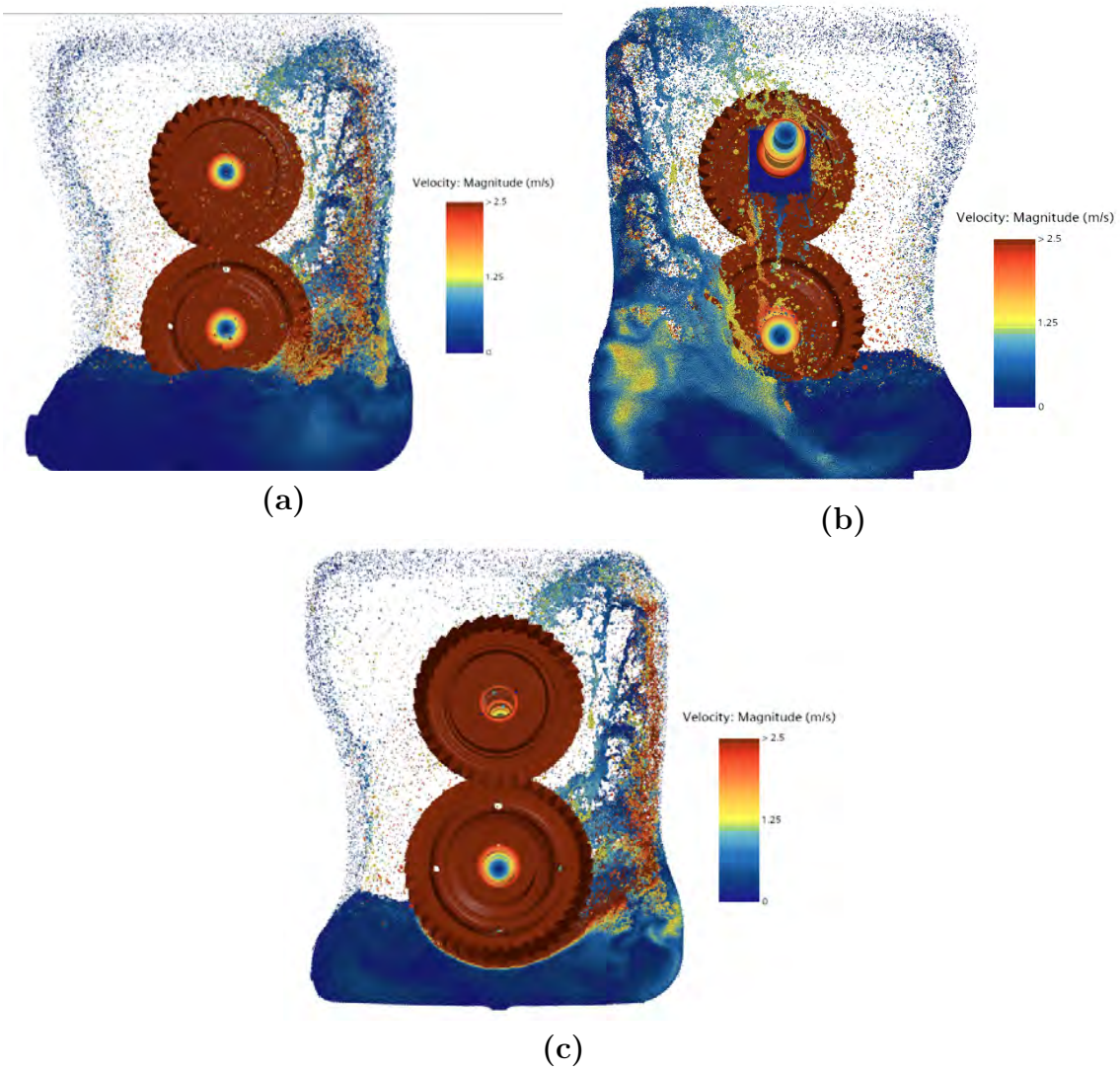


Figure 7.4: REF velocity magnitude of oil flow at 1200RPM:
(a) Front (b) Back (c) Front cross-section

It can be seen that many of the particles have a velocity of $1.25 m/s$ and below. Oil at the bottom of the lower gear is being moved at a high velocity by the teeth. The oil does not have a very defined or fast stream compared to HA+HR and FA+HR; instead, the oil splashes from the right wall and hits the gear wheels from several directions at a relatively slow speed. There is, however, a tendency of faster-moving oil on the right wall at this speed. At the back (Figure 7.4b), the oil pools against the wall as it is being pumped by the lower gear wheel. The direction of the helical teeth is the reason for this flow direction. The front cross-section (Figure 7.4c) shows how the particles are directed slightly up but the definition of the stream quickly fades and becomes more of a mist. Many of the same characteristics remain at 1800 RPM (see Appendix B, Figure B.1).

Figure 7.5 shows the same perspectives for the HA+HR configuration at 1200 RPM.

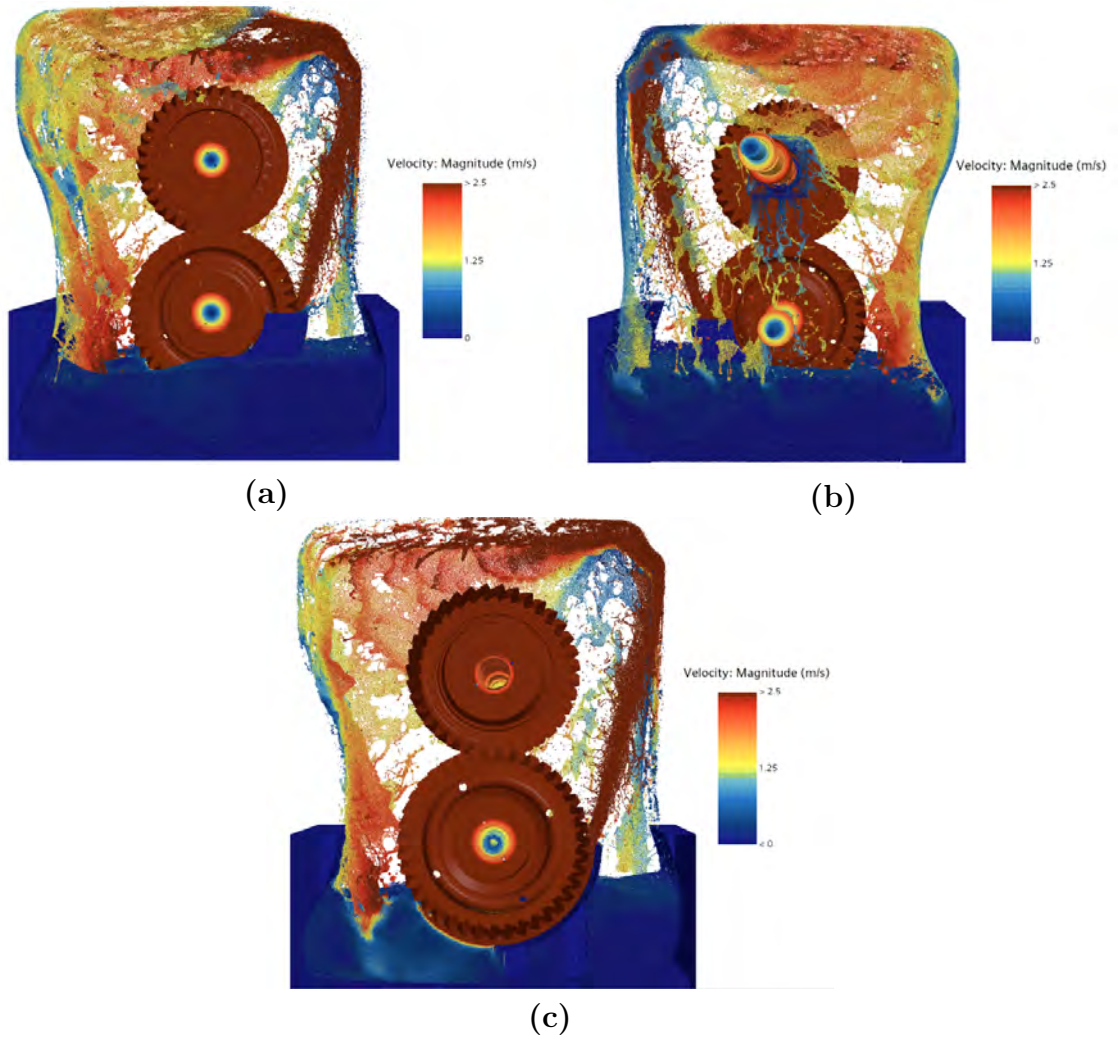


Figure 7.5: HA+HR velocity magnitude of oil flow at 1200RPM:
(a) Front (b) Back (c) Front cross-section

This setup shows a very strong stream of fast-moving oil that flies up on the walls, redirects along the top and finally back down with a slightly slower velocity than it initially had. There is not as much of an oil mist with this configuration. Looking at the back, the oil does still flies towards the back wall but most of it hits the upper right corner at a higher speed (see Figure 7.5b). The cross-section (Figure 7.5c) further visualize how the insertion geometry directs the flow strongly to the top right corner, how it circulates and finally falls back down behind the lower gear (on the left). This creates a pool of oil that moves slightly faster than its surroundings, left of the lower gear. The same characteristics persist at 1800 RPM and are shown in Appendix B, Figure B.2.

The next configuration is FA+HA and can be seen in Figure 7.6.

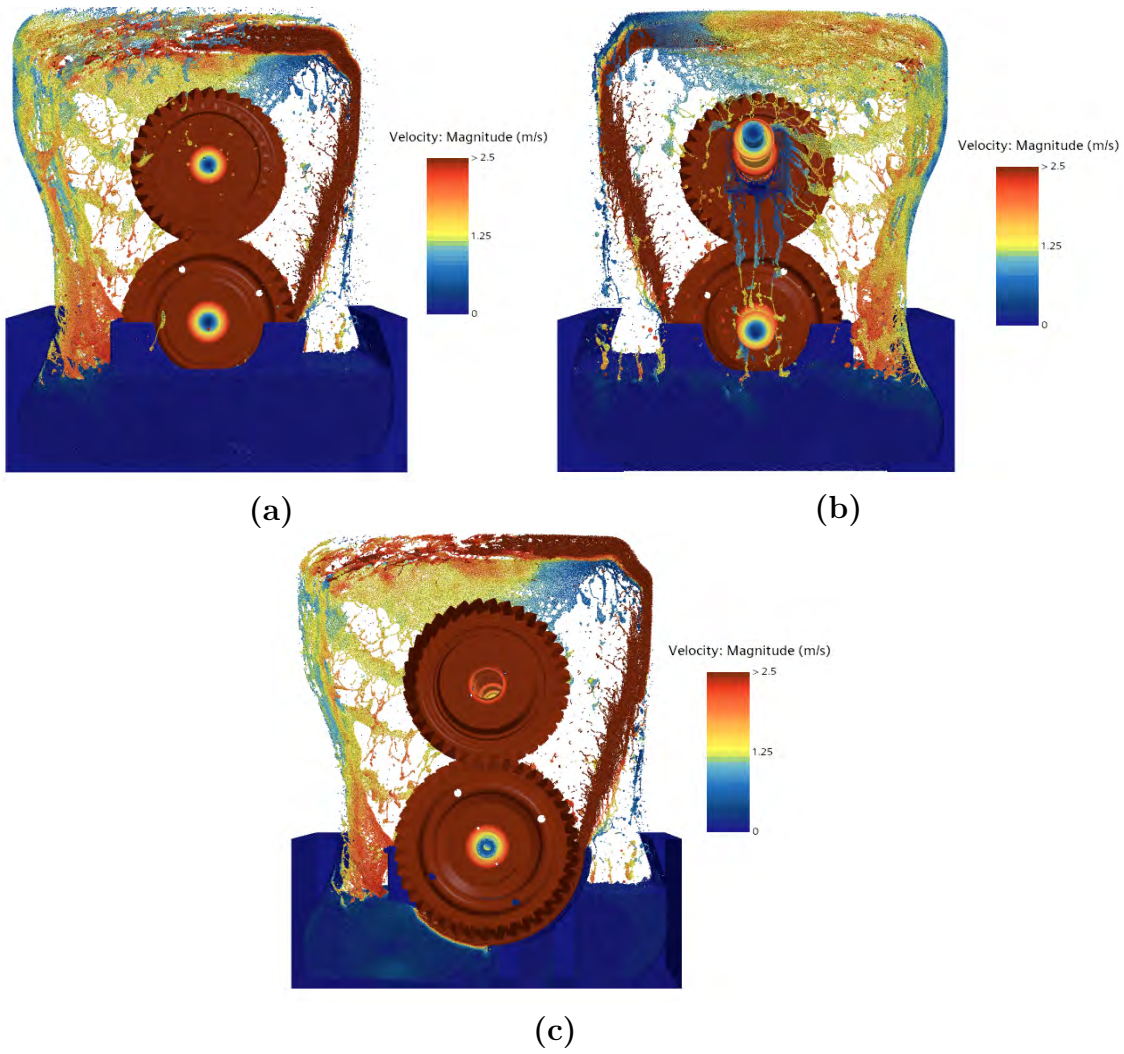


Figure 7.6: FA+HR velocity magnitude of oil flow at 1200RPM: (a) Front (b) Back (c) Front cross-section

In this setup, the strong stream remains and shoots oil up to the right corner of the transmission housing. It then comes back down behind the lower gear wheel. Oil also hits the front of the housing, similar to the HA+HR configuration. However, less oil is hitting the front and back wall and at a lower speed compared to HA+HR. This means that the oil sprays straighter upwards with this configuration. Figures showing the same perspective for this configuration at 1800 RPM are found in Appendix B, Figure B.3.

7.1.3.1 Recirculation

Streamlines visualize how the lower gear wheel is affected by the recirculation of oil in the oil sump and can be seen in Figures 7.7, 7.8 and 7.9. These show streamlines on a plane just below the lower gear wheel at a top view angle.

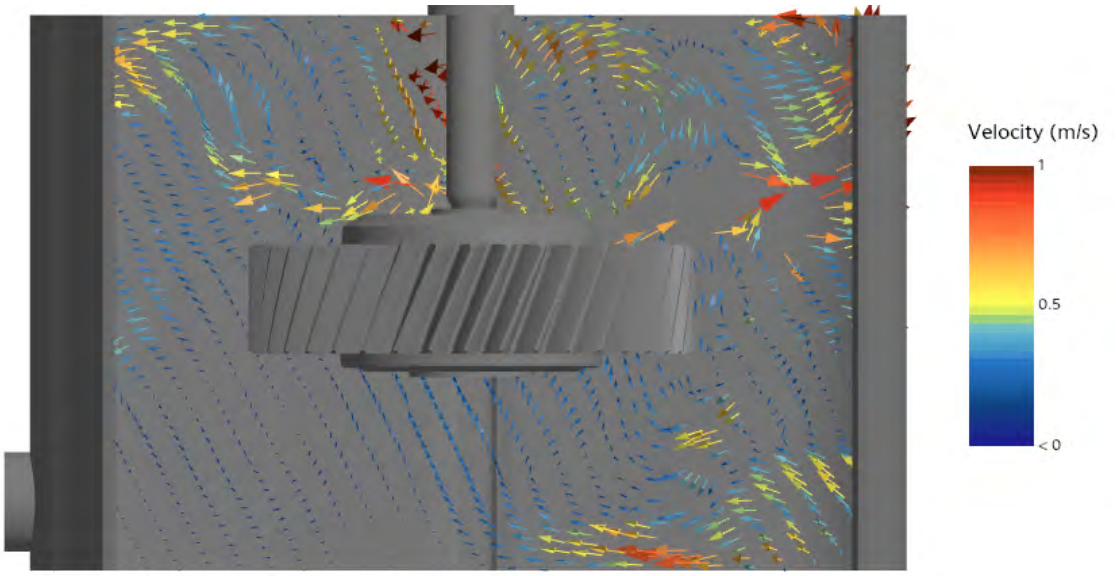


Figure 7.7: Oil flow recirculation of REF at 1200 RPM

The chaotic, unguided flow of the REF seen in Figure 7.4 is further visualized above (Figure 7.7). Oil is being pumped to the top-right corner, as previously seen. However, as oil hits the right wall, it also circulates back around at the lower-right corner and hits the gear from the side. The large pool of oil at the back wall and the oil splash around the top gear create faster-moving streamlines at the top-left corner due to the change in splash direction. This oil then slightly hit the gear from the side before being pumped again.

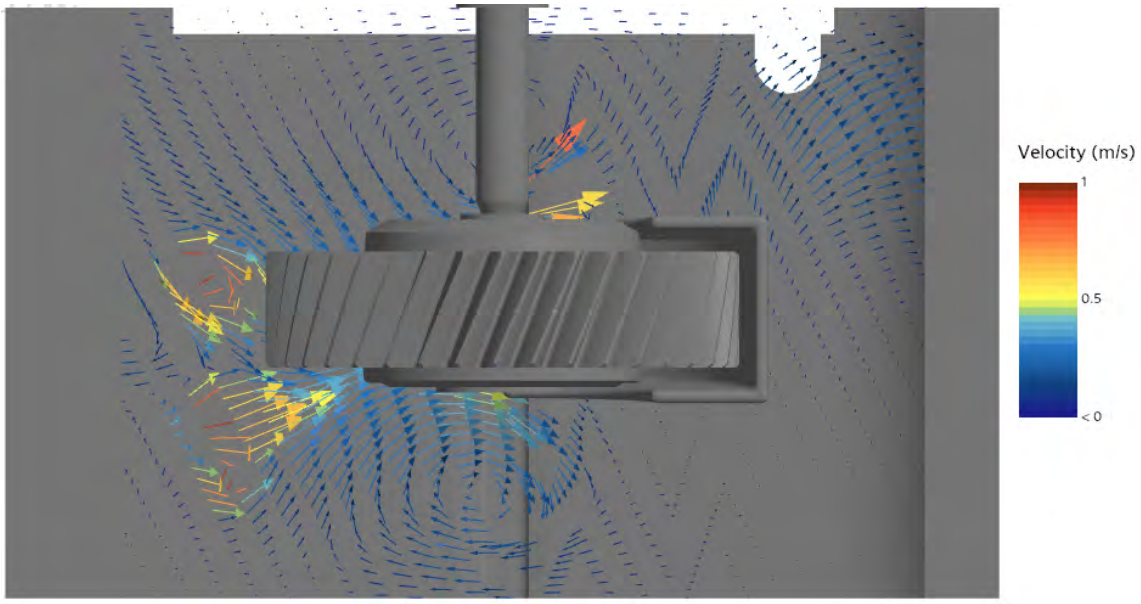


Figure 7.8: Oil flow recirculation of HA+HR at 1200 RPM

Studying the HA+HR configuration (Figure 7.8), the characteristics change drastically. As oil is directed upward by the geometry, it results in slower-moving oil in

the oil sump, especially on the right. Much of the oil splashing around the top (see Figure 7.5) comes back down on the left side. This can be seen by the concentration of faster streamlines in the lower-left corner of the figure. The oil then circulates slightly and hits the gear wheel from the side and back before being pumped again.

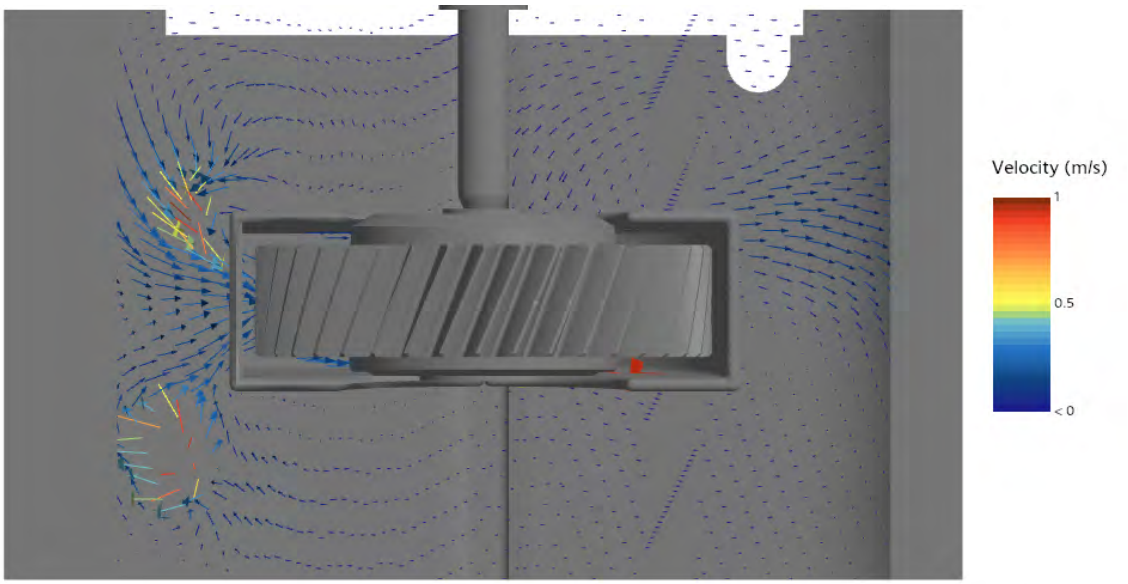


Figure 7.9: Oil flow recirculation of FA+HR at 1200 RPM

The FA+HR configuration (Figure 7.9) keeps much of the slow-moving oil in the sump, like the HA+HR configuration. The extra guidance of the extended axial wall throws the oil almost straight up and around, as seen in Figure 7.6. As this oil splashes down on the left side of the gear, it creates two whirls on the left side of the figure. This oil circulates and is forced through an opening on the back of the geometry. The axial walls prevent most of the recirculating oil from hitting the gear from the side. Streamline figures for 1800 RPM can be found in Appendix B, section B.1.

7.2 Test rig testing

The experimental results are summarized in Figure 7.10. It lists every insertion concept used in the thesis with its relative power loss compared to the reference (P/P_{REF}) at each RPM point. The red bar above each staple shows the standard deviation ratio, calculated using error propagation. This indicates the uncertainty of each measurement.

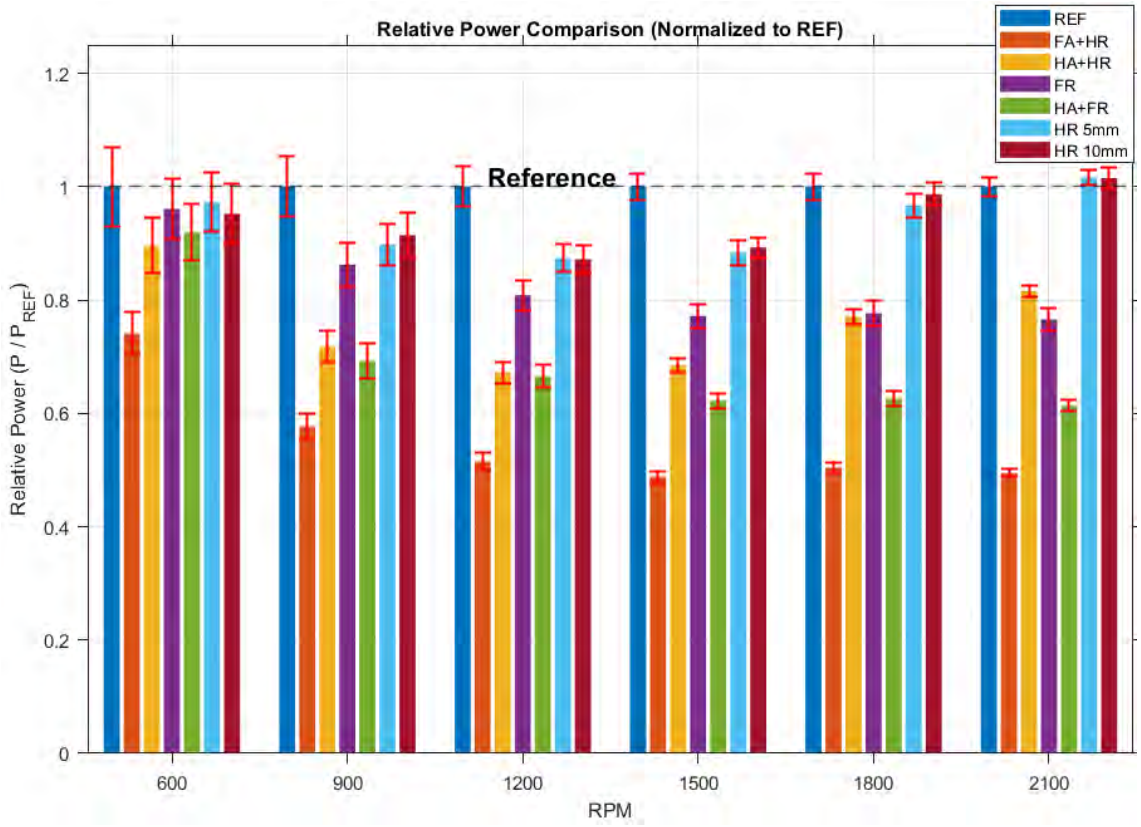


Figure 7.10: Experimental relative power loss for all insertion concepts

At 600 RPM, the differences between most configurations are small and within the measurement uncertainty. However, FA+HR stands out as superior to all configurations, with a measurable performance gain. Increasing the speed to 900 RPM shifts the results slightly. The FR, HR 5mm and HR 10mm are all performing within the uncertainty of each other, while the REF is slightly worse. HA+HR and HA+FR are better and experience approximately the same losses. FA+HR is once again better than all of the above. Insertions using axial walls are now starting to show lower power losses than configurations without. Further increasing the speed to 1200 RPM does not show any significant shift in trends and looks about the same as 900 RPM. However, the gap to the REF has increased slightly.

At 1500 RPM, some slight shifts are starting to form. While the gap between REF, HR 5mm and HR 10mm is holding, the FR configuration is now closing the gap downwards. There are only minor differences between FR, HA+HR and HA+FR at this point. FA+HR still has the lowest losses of all. At 1800 RPM, the difference between REF, HR 5mm, HR 10mm, and the rest is starting to widen. The HR configurations have now shifted upward and are performing at the same level as the REF. HA+FR has separated itself from FR and HA+HR and is showing measurable gains in relation to them. This RPM point also indicates that the full radial wall yields lower losses at higher speeds, which explains why FR decreased as speed increased. However, there is still a gap to FA+HR. This trend continues at 2100 RPM. The full axial wall found in FA+HR consistently performs better than all

insertion concepts at each RPM point. The performance of HR configurations deteriorates at higher speeds as they lose the performance gain to the REF. However, this is improved with the FR configuration, which gains performance with increased speed. There were no meaningful differences in losses between HR 5mm and HR 10mm, indicating that the radial distance to the gear is insignificant at these speeds.

7.2.1 Flow observations

Below are figures of all insertions/configurations running at 600 RPM (Figures 7.11 to 7.16). Starting with the reference (Figure 7.11), the lower gear wheel shoots oil up and slightly towards the back wall (away from the viewer in the figure). The oil then follows the housing wall up and eventually falls behind the upper gear and partially onto it. The oil is moving toward the back wall due to the helical cut gears that are oriented in that direction. As the oil splashes down in the oil sump, air bubbles form evenly under the surface.



Figure 7.11: REF oil flow at 600 RPM

Figure 7.12 shows the FR insertion in use. Here, the oil is distinctly guided upwards by the geometry with a focused spray but it is still also going slightly toward the back wall. Focused meaning how distinctly and coherently the stream of oil shoots up after being pumped by the lower gear. The oil hits the upper right corner of the housing, follows the contour and then falls behind and partially on the upper gear. Air bubbles are forming in the oil sump due to the splashdown of the oil. This happens mostly on the right side of the oil sump.

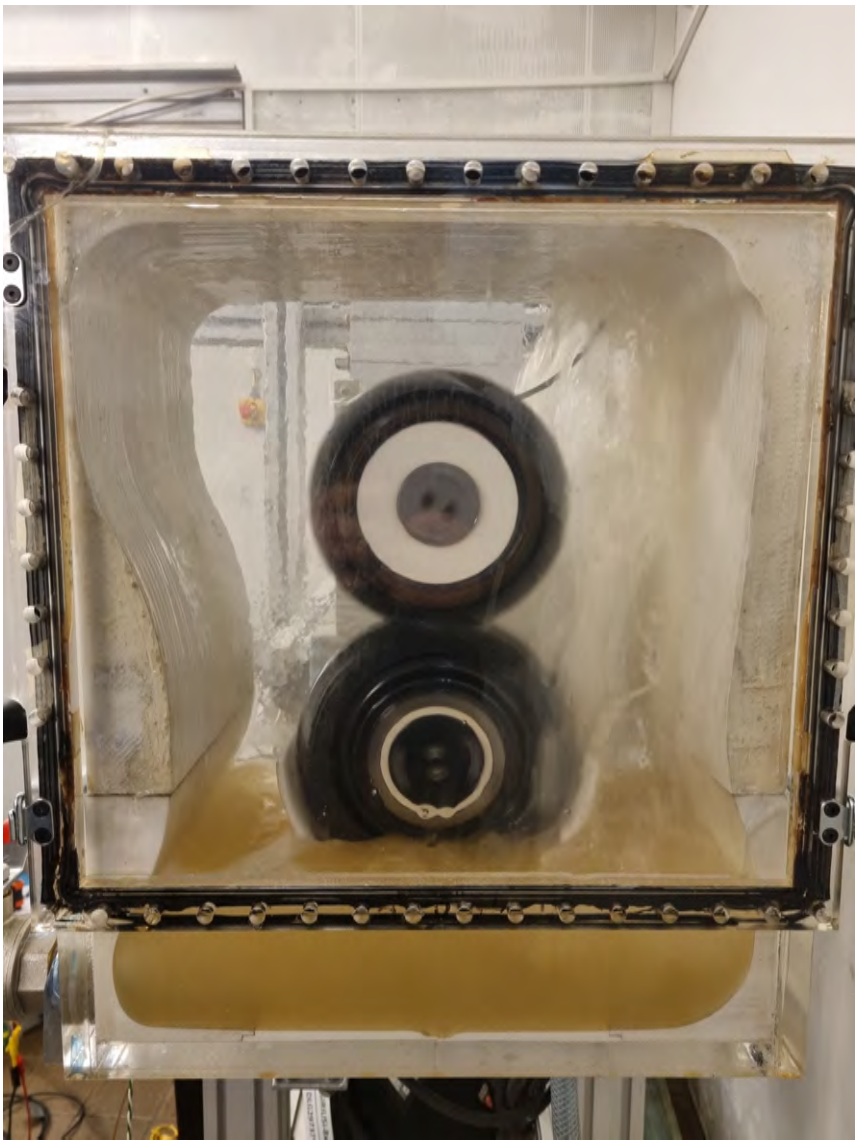


Figure 7.12: FR oil flow at 600 RPM

Figure 7.13 uses the HR insertion. The oil is guided similarly to the previous configuration but with a slightly less focused stream of oil going straight up. This results in more oil hitting the upper gear after splashing from the top of the housing. Air bubbles are forming mostly on the bottom right in this case.

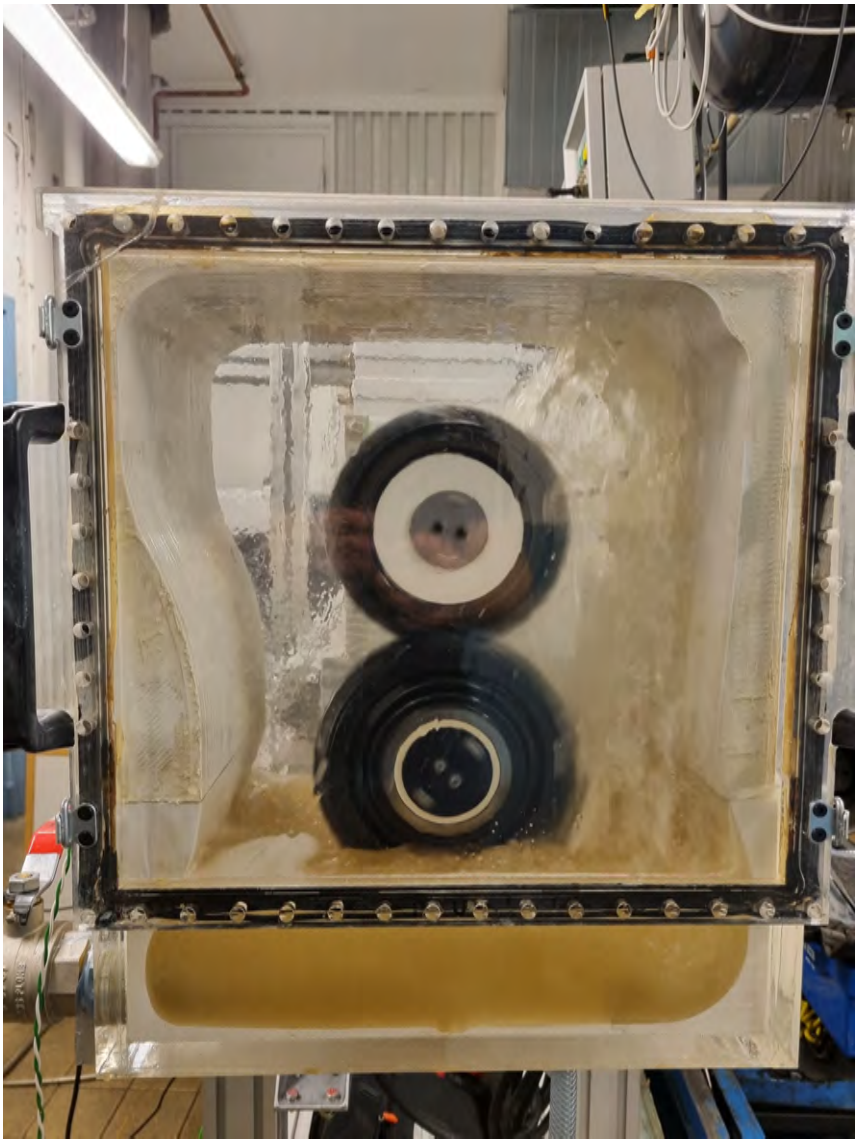


Figure 7.13: HR (5mm and 10mm) oil flow at 600 RPM

The first insertion that utilizes an axial wall is the HA+HR configuration and can be seen in Figure 7.14. The stream direction of the oil splash now changes from the previously mentioned configurations. The stream is still focused and going up but it is instead flying slightly toward the front wall (towards the viewer in the figure). This results in the oil falling in front of the upper gear while still partially hitting it but at a lower rate than before. The air bubbles are forming evenly in the system but with a slight concentration on the right side.



Figure 7.14: HA+HR oil flow at 600 RPM

The HA+FR insertion can be seen in Figure 7.15. As previously discovered, the full radial extension provides a slightly more focused stream than the HA+HR configuration, meaning more oil hits the upper parts of the housing. The direction of the stream remains the same. The splashdown of oil happens mostly in front of the lower gear, with some hitting the upper gear. Bubbles are forming with almost the same characteristics as the HA+HR configuration. Comparing it to the FR configuration, the stream direction is different due to the axial wall but it still appears to have a similar distribution of air bubbles.



Figure 7.15: HA+FR oil flow at 600 RPM

The final insertion concept in Figure 7.16 is the FA+HR configuration. This continues to splash oil up but noticeably less focused compared to the previous configuration. However, the oil is now splashing distinctly toward the front wall and hitting the rig window. This results in almost no oil disturbing the upper gear on the way down (at this RPM). Bubbles are forming mostly on the bottom right, where the oil is splashing down from the window.



Figure 7.16: FA+HR oil flow at 600 RPM

7.3 Simulation vs experimental results

To link the simulation and experimental data, a comparison table is presented (Table 7.1). The error percentage shows how much the simulated value differs from the experimental one (P_{sim}/P_{test}), with (+) indicating an overestimation and (−) indicating an underestimation.

Table 7.1: Comparison of simulated and experimental power loss

Configuration	**RPM**	**Error [%]**
REF	1200	−25%
REF	1800	−10%
HA+HR	1200	+73%
HA+HR	1800	+64%
FA+HR	1200	+37%
FA+HR	1800	+55%

The reference is the closest, with a simulated power loss of −10% at 1800 RPM and −25% at 1200 RPM, compared to the tests. However, the trend toward underestimating power losses is inconsistent, and the remaining configurations severely overstate simulated power losses. The HA+HR configuration shows +73% and +64% at 1200 and 1800 RPM, respectively. FA+HR continues this overestimation and shows +37% and +55% at the two RPM points. This shows that the actual simulation values of the losses are not reliable, since they differ substantially from reality.

8

Discussion

This thesis aims to provide further knowledge regarding splash churning losses in Volvo's AMT gearboxes and to create a guide that aids future transmission housing designs. It also investigates how different geometries/insertions within the transmission housing affect churning losses, using both simulations and experimental tests. This chapter will discuss and interpret the simulation and experimental results. It will also evaluate how well the simulation data match the experimental data.

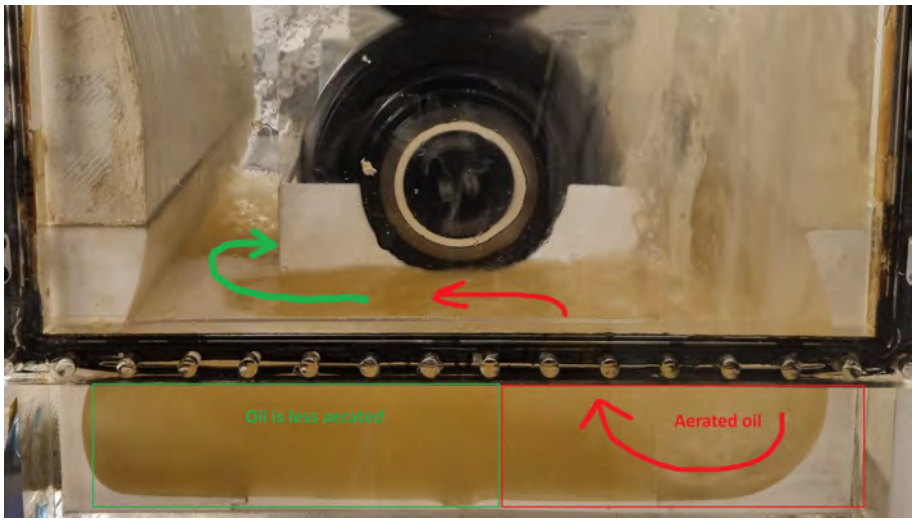
The comparison in Table 7.1 showed that the simulation model did not reproduce the experimental trends with sufficient accuracy. The reference showed that the simulated power loss is within 10% of the tests at 1800 RPM but already underestimated losses by -25% at 1200 RPM. For the insertion concepts, the error was even larger and with an opposite sign. HA+HR and FA+HR consistently overpredicted the power losses by 37-73% across both RPM points. This combination of results indicated that the simulation model was not robust to geometry changes inside the housing and therefore, cannot be considered reliable for predicting absolute churning losses. As a result, the simulations were mainly useful for identifying recirculation trends in the sump rather than providing accurate loss predictions. A possible source of this error could be the use of a single-phase simulation model. The models used in the project only simulated oil and excluded air. Air in the system has the potential to shift the results to more realistic values.

Another important point to discuss, is that the trends found during testing were not consistent with the simulated trends. Although FA+HR performed the best like the testing, HA+HR was substantially worse than the REF (see Figure 7.2). There were attempts to locate the source of losses by studying streamlines in different planes but no anomalies were found. This would indicate that the simulation model cannot be trusted for studying trends between insertions either, at least not with a 1-phase system using 1mm particles. It could also be linked to how the flow behaved in the simulations. It was observed that the particle flow did not match the experimental flow observations very well. The particles seemed to splash aggressively around the top of the housing and around the upper gear wheel when using insertions. This splash behavior was not present during testing. Although the direction of the splash matched the testing when using the REF and HA+HR, FA+HR's splash direction was completely different in the simulation, with the fluid splashing almost vertically instead of toward the front wall. Possibly linked to particle size and the lack of a 2-phase system. Consequently, the most interesting flow to study from the simulations was how the recirculation behaved and was affected by the ax-

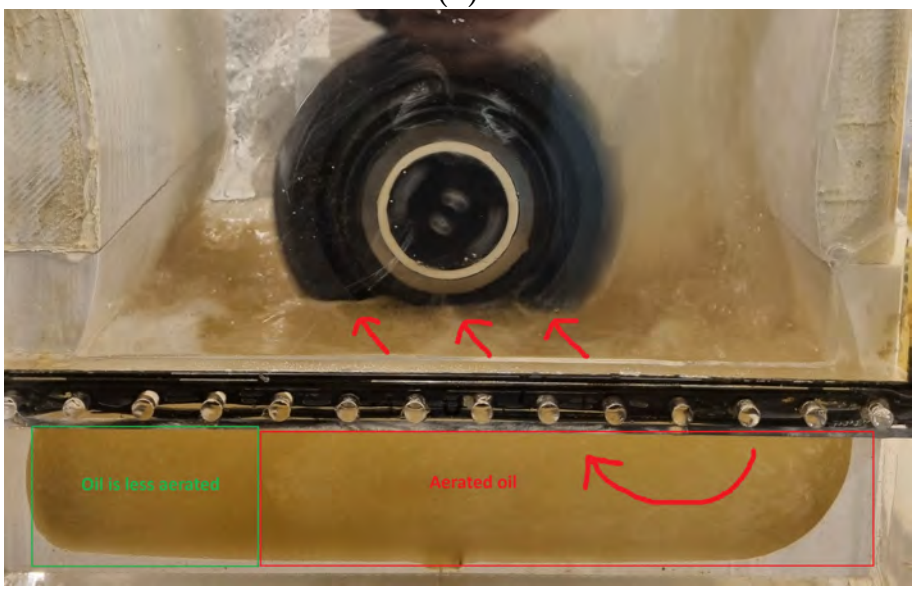
ial insertion geometry (see subsubsection 7.1.3.1). It was found that the axial walls (in combination with the radial geometry) seemed to redirect and shield the lower gear from opposing forces/streamlines of oil. Instead, the oil was forced to round the axial wall before being pumped by the lower gear again. This was especially visualized in Figure 7.9 where most oil entered through the back of the insertion geometry. On the contrary, Figure 7.7 showed the re-circulation of the REF. This showed that the unguided flow of the reference meant that more of the recirculating oil seemed to impact the lower gear from the sides, possibly leading to more losses due to opposing forces. These flow trends were present for both 1200 and 1800 RPM.

From section 7.2, the observed relative power loss changes with RPM. At 600 RPM the power reading is small, often not exceeding $15W$. This, in combination with the limited splashing at this speed, is most likely why no major improvements are observed compared to the reference. However, increasing the speed to 900 RPM shows larger differences between the various configurations. The relative power readings then level off and remain consistent across most insertion concepts. This is probably due to the flow reaching a state that consistently affects churning losses in the same manner for all RPM points. The exceptions to this observation are HR (5mm and 10mm) and HA+HR. The performance of these insertions deteriorates after 1500 RPM and instead, they increase in relative power. The common denominator among these three is the half radial wall. A possible explanation for why this happens is that the half radial wall might create a disturbance at the bottom of the lower gear, which could abruptly affect the oil with no smooth transition. This theory is further reinforced by the FR and HA+FR insertions that do not exhibit this behavior.

The results in Figure 7.10 show clear trends linked to different geometrical features of the insertions. Immediately after 600 RPM, two groups of insertions have formed. The upper group consists of FR and HR (5mm and 10mm) and these insertions do not have any axial walls. HA+FR, HA+HR and FA+HR make up the lower group and all include axial walls. While all provide measurable performance gains between 1200 and 1500 RPM, the axial walls provide better results. This is possibly linked to how the flow is directed to the right, unlike the insertions without axial walls (see subsection 7.2.1). Another possible explanation is that the axial wall might shield the lower gear wheel from recirculating aerated oil/bubbles, which cause losses due to poorer lubrication and cooling characteristics. Figure 8.1 shows the hypothetical aerated oil path for FA+HR and REF based on flow observations. Looking at the FA+HR configuration, most bubble formation appears to happen on the right side. The more chaotic flow of the REF configuration seems to have a larger, evenly distributed aerated area. This larger area, along with an open path axially to the lower gear (indicated by red arrows), would mean the gear is exposed to more aerated oil. On the contrary, the FA+HR configuration has a full axial wall. This wall could theoretically stop the initial aerated oil from reaching the lower gear and instead redirect it to the left in the figure (see red arrows). This would give the oil more time to release air and improve its cooling characteristics before entering through the opening in the back (see green arrow) while also shielding from any opposing forces from recirculating oil.



(a)



(b)

Figure 8.1: Hypothetical oil path or aerated oil:
(a) FA+HR (b) REF

This would explain why FA+HR insertion consistently achieves better results than the others, since it is the only insertion with full axial coverage. It also shows that it would be interesting to test a full axial configuration without any radial geometry. Something that the time scope of this thesis could not cover, as the number of possible combinations was limited by the concept matrix early on.

From the observations under subsection 7.2.1, losses also seem to stem from how much of the oil splash hit the upper gear. The best insertion concept is the FA+HR, as stated before. This configuration experiences fewer oil splashes on the upper gear than others, possibly explaining its low losses. However, less oil splashing on the upper gear might cause cooling problems in real applications and should be considered before use.

In Figure 7.10, error bars are visualized as red bars on top of each staple. These stem from the standard deviation of all data collection runs, at all RPM points and for each configuration. The biggest contributors to these uncertainties are probably the difference in oil temperature and the slight RPM differences. A typical data collection starts with the oil at about 20°C and ends at about 25°C (after 48 data collection points). This temperature difference changes the viscosity of the oil and might slightly affect the data. The electric motor speed (RPM) is controlled through an ESC (Electronic Speed Controller). These settings are kept consistent and are verified by the speed sensor in the test rig. Only minor fluctuations are observed and rarely exceed ±4 RPM. However, this might still affect the data. But consistent results from the reference (REF) tests conducted before and after the insertion tests support the reliability of the experimental setup.

Future work

Future work should focus on implementing a 2-phase SPH model that includes both air and oil. This would enable a more realistic representation of the test rig by better representing oil aeration and hopefully, flow behavior. It should also investigate whether lowering the particle size has any meaningful impact on power loss and flow compared to experimental testing. Of course, this would increase calculation time significantly and is something to consider. If an improved model can be created, the simulations should explore more insertion concepts while also widening the RPM range.

The insertions tested in this work provide a first indication of potential efficiency gains, however, there is still room for further geometry optimization. Further studies should focus on refining insertions through systematic design via experiments and/or simulations (provided that a sufficient representation model is created). This design process could investigate more complex geometrical differences rather than being limited to simple axial/radial geometries. A process that could lead to even larger performance gains.

Building on the previous paragraph, high-speed camera equipment for the test rig should be used to better understand the flow behavior inside the transmission housing. Such equipment would enable direct observation of splash patterns, recirculation in the oil sump and aerated regions for different insertions. Correlating this with measured losses could provide an even better qualitative understanding of the flow and possibly the root of the losses.

The thesis primarily focused on churning losses, while cooling performance and aeration have only been discussed qualitatively. Future studies should therefore investigate how different insertion geometries affect oil temperature distribution, gear cooling and degree of aeration. This could include multiple temperature sensors in the test rig (only one used in this thesis), density based sensors (measuring aeration) or thermal CFD analyzes. This would create a more complete assessment of the different insertion configurations and ensure that they do not compromise cooling performance. An investigation like this would require a test rig that can simulate load.

Finally, future work should focus on practical application of the promising insertion concepts in a full gearbox. As the geometries change the flow behavior and splash direction, it would be interesting to investigate how it could affect different components and gear pairs within the transmission. This is to ensure that the observed efficiency gains are kept in a practical application and can be made in to a feasible feature of the AMT gearbox.

Conclusion

This study investigated how different insertion geometries affect splash churning losses in Volvo's AMT gearboxes using both SPH simulations and experimental testing. It also evaluated how well the simulation data match their experimental counterparts.

The quantitative comparison between simulations and experiments showed that the single-phase SPH model was not robust enough for predicting churning losses and trends, especially when altering the geometry inside the transmission housing. The results were therefore primarily used to understand flow behavior and how insertion geometry affected re-circulation, while the experimental testing served as an indication of the absolute performance of each insertion concept. The lack of a 2-phase system and a resolution size of 1mm particles might be the possible source of the large observed trend and power loss errors between simulations and experimental testing.

Through experimental testing, it was found that the use of insertion geometries inside the AMT transmission housing can yield significant efficiency gains depending on configuration. Clear trends formed after 600 RPM where the insertions were divided by geometrical features. The less efficient upper group consisted of insertions without axial walls and the more efficient group utilized axial geometry. The difference in losses between the groups slightly increased until 1500 RPM where it stagnated. From there, three configurations broke the trend (HR (5mm and 10mm) and HA+HR) and their performance deteriorated with increasing RPM. On the contrary, insertions utilizing a full radial wall were resistant to this increase in speed. This type of geometry also provided a more focused oil spray compared to a half radial wall. The largest efficiency gains relative to the reference were observed with the FA+HR configuration. This insertion consistently performed better than the rest across all RPM points and showed the importance of a full axial wall. These trends were observed for the tested RPM range of 600 to 2100 RPM at a constant oil level and temperature of 20 to 25°C. The measured losses between the different configurations exceeded the estimated uncertainty, indicating that the trends are robust.

Another discovery was that the difference in radial distance to the gear did not have any meaningful impact on the measured losses. Instead, the radial geometry's main function was to redirect oil flow. Continuing with the oil flow observations found in subsection 7.2.1, the causes of losses could be discussed qualitatively. Although not quantified in this work, it was theorized that losses stemmed from the amount of oil impacting the upper gear and/or from aerated oil in the system.

Declaration of AI use

In this work, ChatGPT, Claude, Gemini and Grammarly's Superhuman Go have been used in different stages of the thesis. To summarize, the tools have mostly been used to correct grammar, help with clarity in texts, generate code for plots and tables, and brainstorm different discussion topics. The material has been scrutinized and fact checked by me to ensure factual and correct statements. All generated material has been reworked before being used in the report. I take full responsibility for the final contents of this thesis.

Bibliography

[European Commission, 2023] European Commission, Revision of the CO_2 emission standards for Heavy-Duty Vehicles. https://ec.europa.eu/commission/presscorner/detail/en/qanda_23_763

[Holmberg et al., 2014] K. Holmberg, P. Andersson, N.-O. Nylund, K. Mäkelä, and A. Design and evaluation of a test rig for measuring gear related losses within a Volvo Trucks gearbox (2014) Global energy consumption due to friction in trucks and buses. Tribology International, 78, pp. 94–114. https://www.sciencedirect.com/science/article/abs/pii/S0301679X14001820

[Opdam, 2023] W. Opdam (2023) Experimental Investigation of the Influence of a New Volvo Trucks Gear Design on the Load-independent Churning Losses Inside a Gearbox. Master Internship Report, Department of Mechanical Engineering, Power and Flow Group.

[Shao et al., 2026] S. Shao, E. A. Hartono, X. Lang, X. Xia, Z. Chen, F. Wei, C. Zhou, and V. Chernoray A comparative study on oil flow and bubble distribution characteristics of FZG gear and cylinder gear. Faculty of Transportation Engineering, Kunming University of Science and Technology, China; Department of Mechanics and Maritime Sciences, Chalmers University of Technology, Sweden; College of Rail Transit, Chengdu Vocational & Technical College of Industry, China.

[Hartono, 2014] E. A. Hartono (2014) Study of Fluid Flow Inside the Gearbox. Department of Applied Mechanics, Division of Fluid Dynamics, Chalmers University of Technology, Gothenburg, Sweden. https://research.chalmers.se/publication/205398/file/205398_Fulltext.pdf

[Hartono, 2019] E. A. Hartono (2019) Experimental Study on Truck Related Power Losses: The Churning Losses in a Transmission Model and Active Flow Control at an A-pillar of Generic Truck Cabin Model. Chalmers University of Technology. https://www.cfd-sweden.se/lada/MoF-old/postscript/PhD-thesis-erwin.pdf

[Changenet and Velex, 2008] C. Changenet and P. Velex (2008) Housing influence on churning losses in geared transmissions. Journal of Mechanical Design, 130(6), 062603. https://asmedigitalcollection.asme.

org/mechanicaldesign/article-abstract/130/6/062603/470496/Housing-Influence-on-Churning-Losses-in-Geared

[Andersson, 2014] M. Andersson (2014) Churning losses and efficiency in gearboxes. Licentiate Thesis TRITA–MMK 2014:11, Department of Machine Design, KTH Royal Institute of Technology, Stockholm, Sweden. https://www.diva-portal.org/smash/get/diva2:752030/FULLTEXT01.pdf

[CarTechBooks, 2015] CarTechBooks (2015) Manual Transmissions Explained. CarTechBooks Tech Tips. Available: https://www.cartechbooks.com/blogs/techtips/manual-transmissions-explained?srsltid=AfmBOooDE_VMOh4sr0awgzNrcYJM7CLs5jJDPOIKx0UPxvJ5ItfEaEGR

[Volvo Trucks, 2026] Volvo Trucks, I-Shift transmission. https://www.volvotrucks.us/trucks/powertrain/i-shift-transmission/

[Volvo Trucks, 2022] Volvo Trucks (2022) AT2812 I-Shift automated gearbox fact sheet. https://stpi.it.volvo.com/STPIFiles/Volvo/FactSheet/AT2812_Eng_01_331482018.pdf

[Volvo Group, 2026] Volvo Group, Climate strategy. https://www.volvogroup.com/en/sustainability/climate-goals-strategy.html

[Liu et al., 2018] H. Liu, T. Jurkschat, T. Lohner, and K. Stahl (2018) Detailed Investigations on the Oil Flow in Dip-Lubricated Gearboxes by the Finite Volume CFD Method. Lubricants, 6(2), 47. https://www.mdpi.com/2075-4442/6/2/47

[Deardorff, UNC] J. Deardorff, Measurement & Uncertainty Analysis Guide. Department of Physics and Astronomy, University of North Carolina at Chapel Hill. https://users.physics.unc.edu/~deardorf/uncertainty/UNCguide.pdf

[Dong et al., 2022] X. Dong, G. Hao, and R. Yu (2022) Numerical investigation of water droplet impact on horizontal beams. Engineering Applications of Computational Fluid Mechanics, Taylor & Francis. https://www.tandfonline.com/doi/full/10.1080/19942060.2022.2026820

[DiveCAE, 2020] DiveCAE (2020) Basics of Smoothed Particle Hydrodynamics (SPH) Explained. https://www.divecae.com/blog/sph-basics

[Formlabs, 2021] Formlabs (2021) What is Selective Laser Sintering (SLS)? https://formlabs.com/blog/what-is-selective-laser-sintering/?srsltid=AfmBOopkweuAbjl4EmcNLAHq_d2_0JvwL3mzNX54RIBK8Mrg9EhYGb1X

[Fransson and Eliasson, 2021] A. Fransson and S. Eliasson (2021) Design and evaluation of a test rig for measuring gear related losses within a Volvo Trucks gearbox. Master's Thesis, Applied Mechanics (MPAME), Chalmers University of Technology, Gothenburg, Sweden. https://odr.chalmers.se/items/04659501-5756-4184-8388-393defed4181

[Q8Oils, 2026] Q8Oils, Q8 Gear Oil V LD 75W-80. Fully synthetic long-drain transmission fluid for heavy-duty gearboxes. https://www.q8oils.com/product/q8-gear-oil-v-ld-75w-80/

[Analog Devices, 2021] Analog Devices (2021) The Basics of Thermocouples. https://www.analog.com/en/resources/design-notes/the-basics-of-thermocouples.html

A

CAD

This chapter contains everything linked to CAD that is not listed in the main report. Figure A.1 shows an early concept of how a possible insertion could be mounted on the lower part of the transmission housing. The yellow legs slot into the housing and the insertion is locked in place.

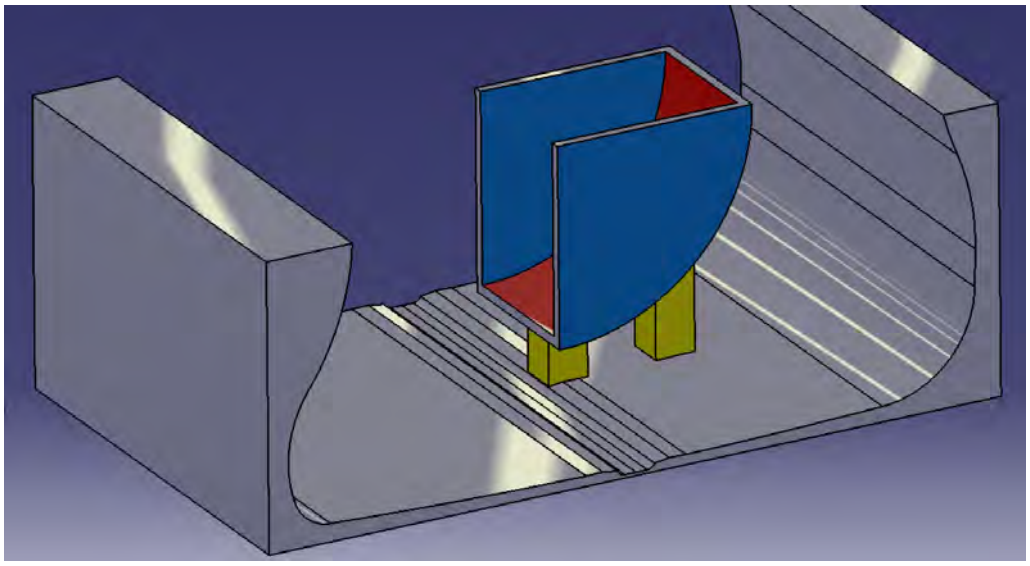


Figure A.1: Mounting concept where inserted geometry is separated from lower housing

Figure A.2 shows how the insertion geometries and lower housing wall were modified before 3D printing. They were split into smaller parts, making the insertions easier to change.

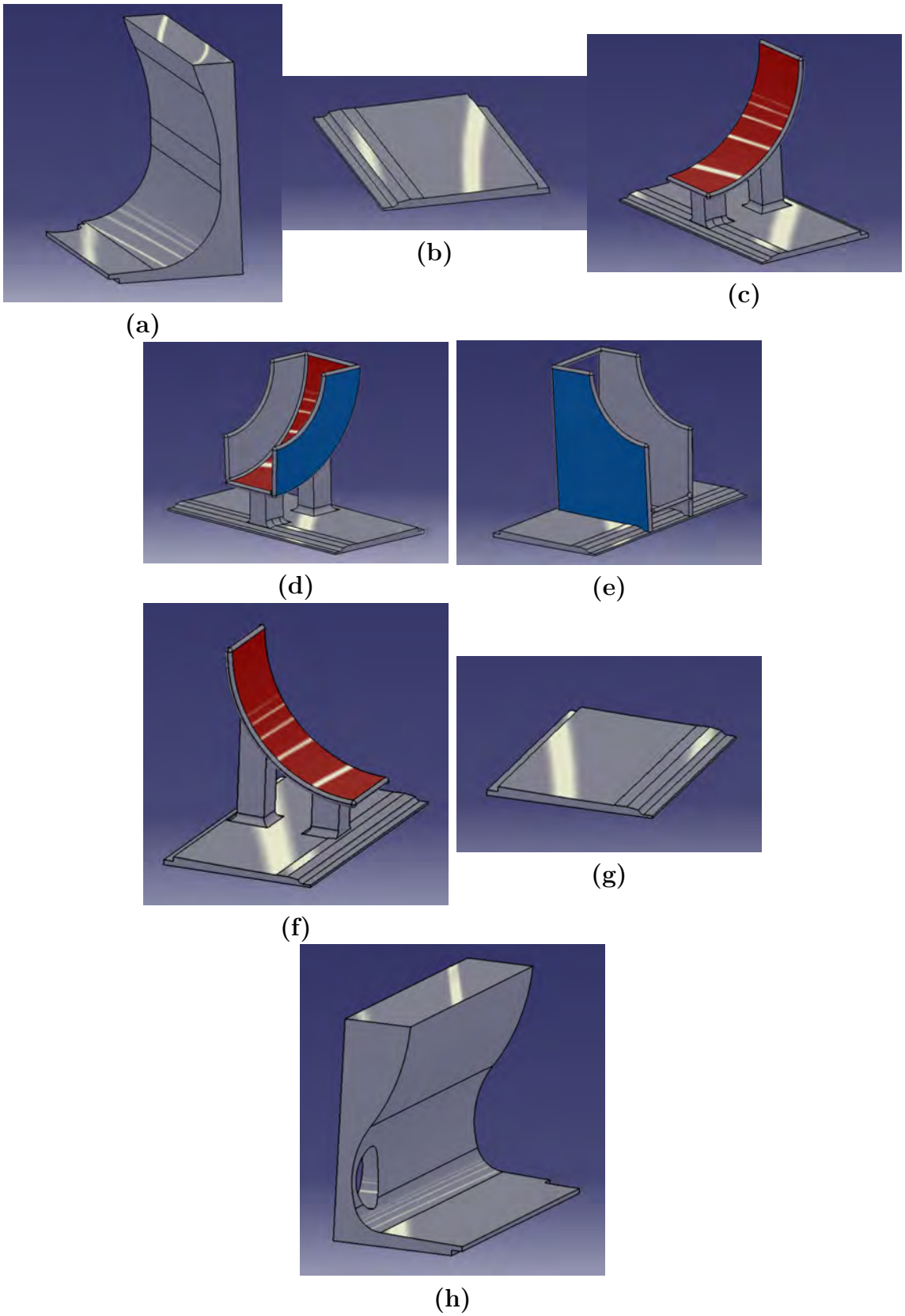


Figure A.2: Divided parts of lower transmission housing: (a) Right wall, (b) Right empty plate, (c) Right radial insertion, (d) Right radial + axial insertion, (e) Left axial insertion, (f) Left radial insertion, (h) Left empty plate, (g) Left wall.

B

Simulation and testing

This chapter contains everything related to simulations and testing that is not listed in the main report.

B.1 Simulation

This section presents flow plots gathered from simulations. It includes front, back and cross-section views of the REF, HA+HR and FA+HR configurations. It also presents streamline figures showing oil recirculation for the same configurations. Figures B.1-B.3 show velocity magnitude plots illustrating the oil splash patterns for 1800 RPM previously referenced in subsection 7.1.3.

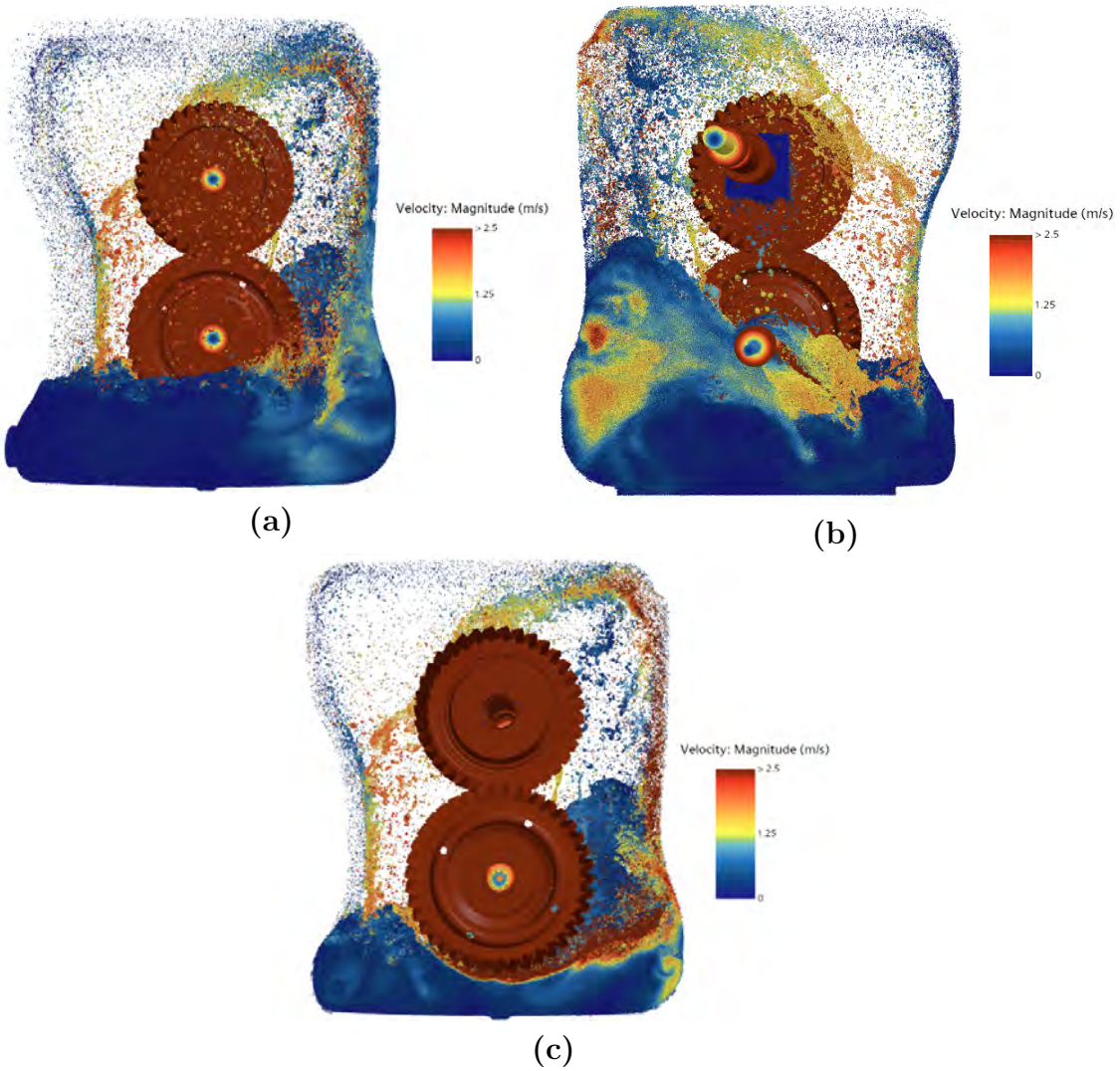


Figure B.1: REF velocity magnitude of oil flow at 1800RPM: (a) Front (b) Back (c) Front cross-section

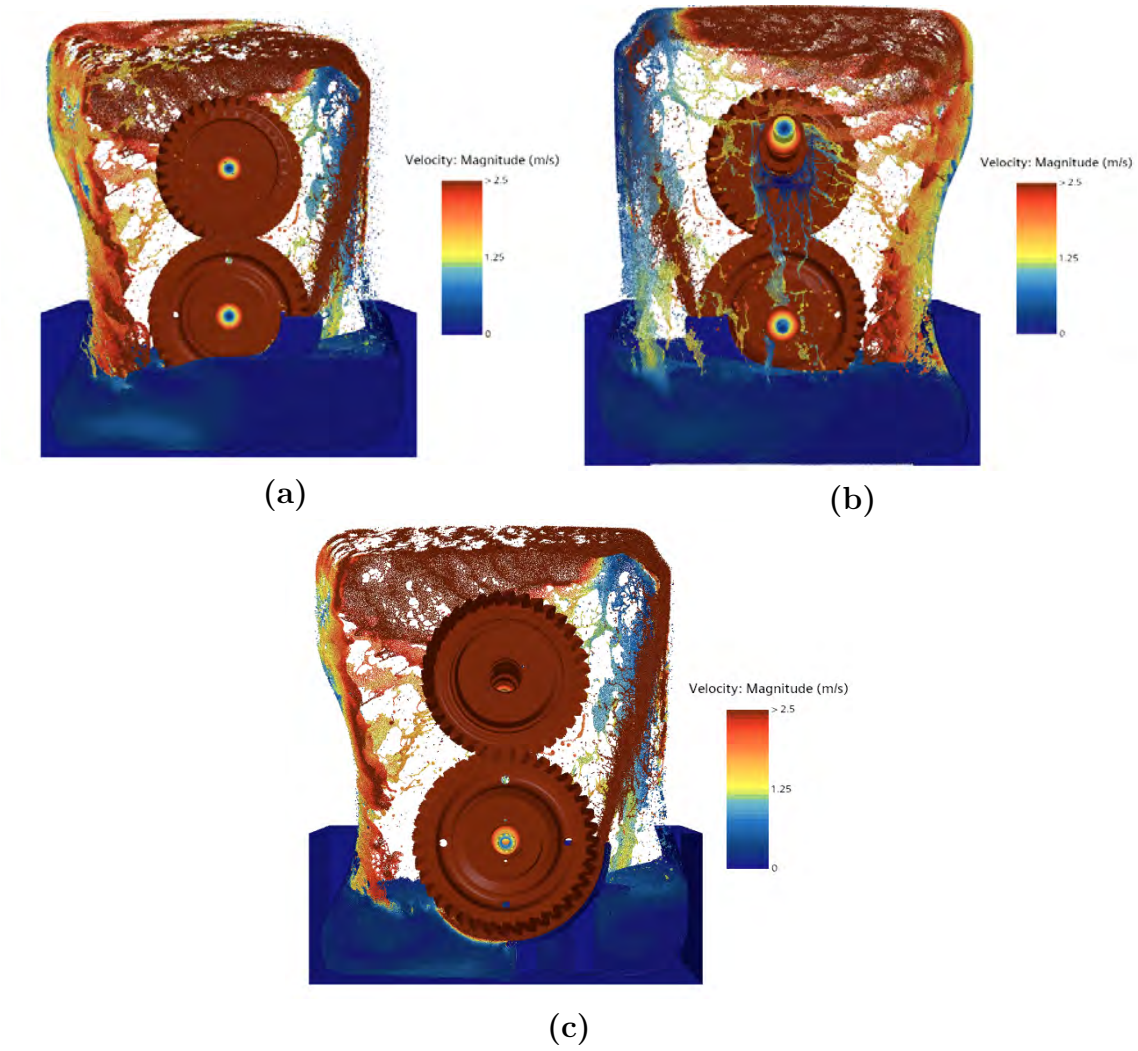


Figure B.2: HA+HR velocity magnitude of oil flow at 1200RPM: (a) Front (b) Back (c) Front cross-section

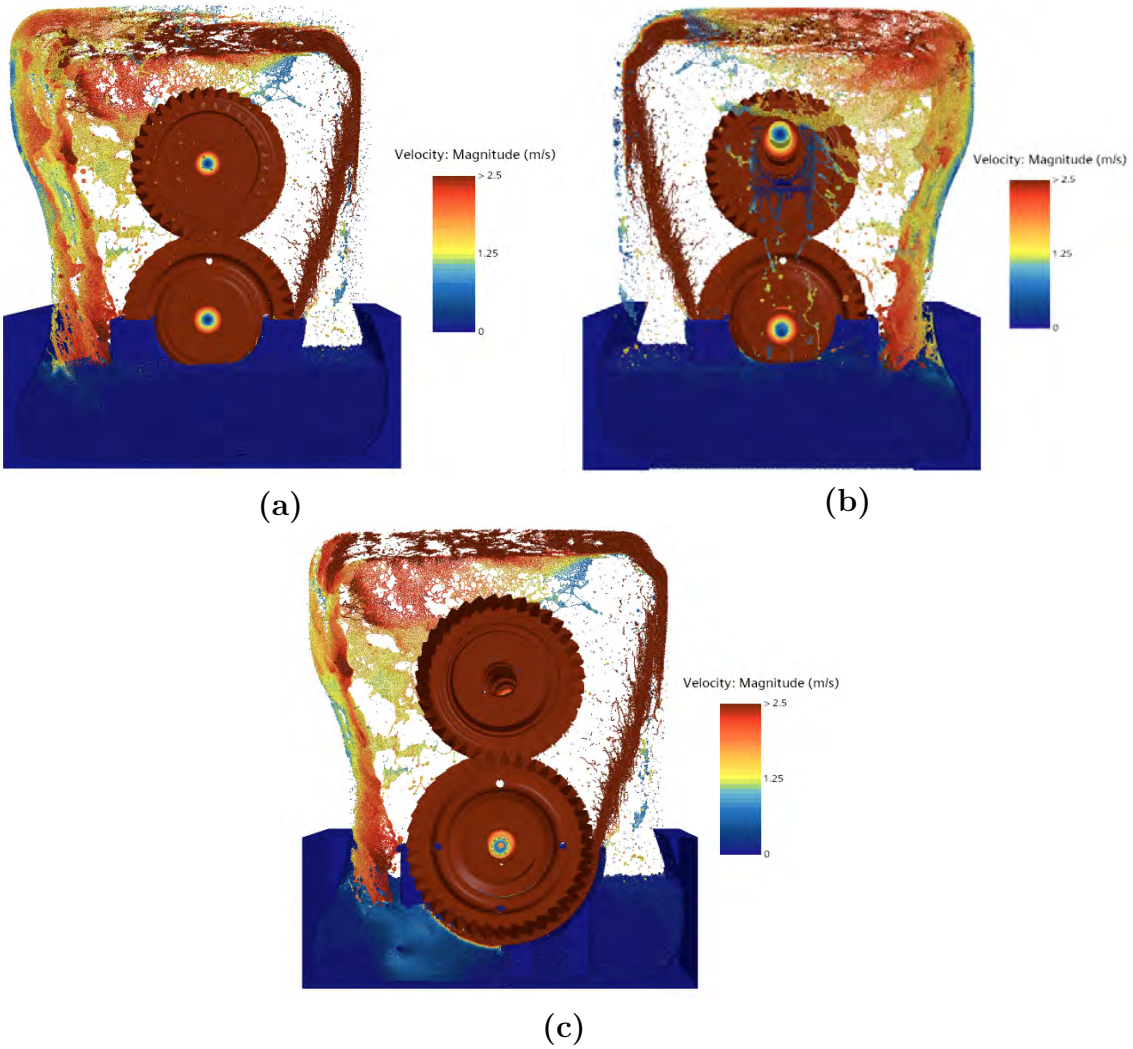


Figure B.3: FA+HR velocity magnitude of oil flow at 1200RPM: (a) Front (b) Back (c) Front cross-section

Figures B.4-B.6 show streamline plots illustrating the oil recirculation patterns for 1800 RPM referenced in subsubsection 7.1.3.1.

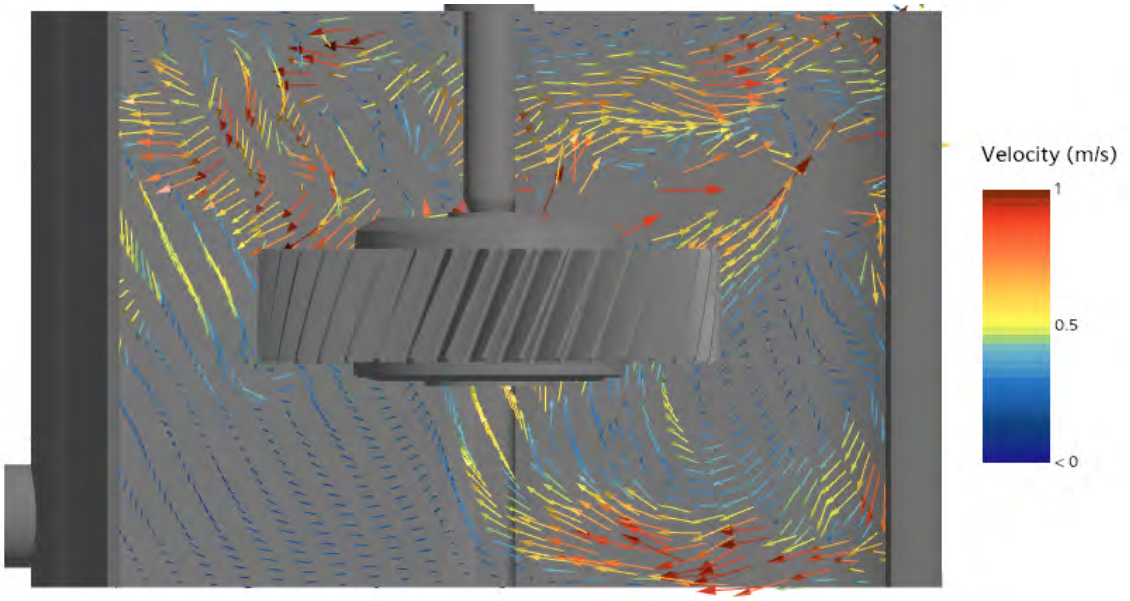


Figure B.4: Oil flow recirculation of REF at 1800 RPM

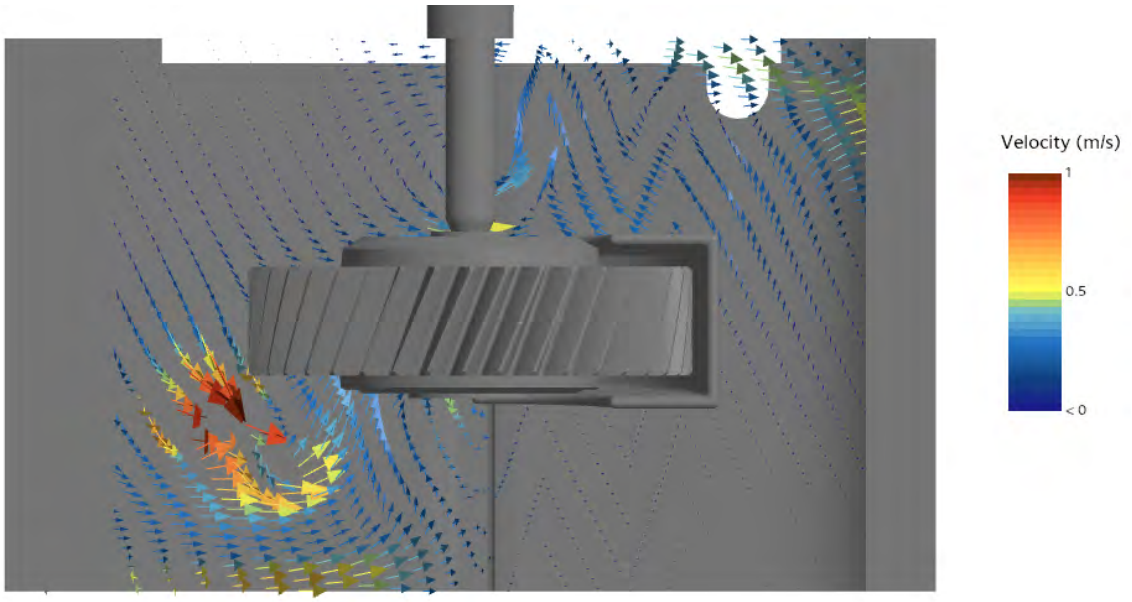


Figure B.5: Oil flow recirculation of HA+HR at 1800 RPM

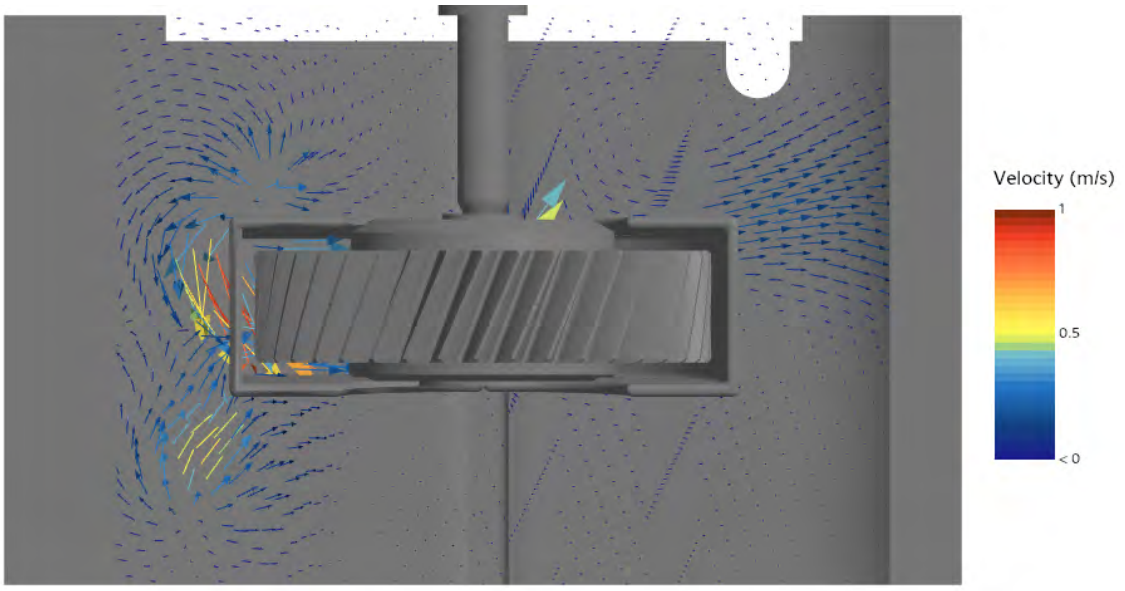


Figure B.6: Oil flow recirculation of FA+HR at 1800 RPM

The schematic of the full test procedure is shown below; each configuration is run 4 times, beginning with the reference. The testing ends with a validation of the results by re-testing the reference. This ensures that the rig has not degraded and that the results can be trusted. Each data record is performed for at least 15 seconds when the values stabilize.

B.2 Testing

33	RPM:	600	900	1200	1500	1800	2100	2100	1800	1500	1200	900	600
34	Ref												
35													
36													
37													
38	RPM:	600	900	1200	1500	1800	2100	2100	1800	1500	1200	900	600
39	HA_HR_D5												
40													
41													
42													
43	RPM:	600	900	1200	1500	1800	2100	2100	1800	1500	1200	900	600
44	HA_FR_D5												
45													
46													
47													
48	RPM:	600	900	1200	1500	1800	2100	2100	1800	1500	1200	900	600
49	FA_HR_D5												
50													
51													
52													
53	RPM:	600	900	1200	1500	1800	2100	2100	1800	1500	1200	900	600
54	FR_D5												
55													
56													
57													
58	RPM:	600	900	1200	1500	1800	2100	2100	1800	1500	1200	900	600
59	HR_D5												
60													
61													
62													
63	RPM:	600	900	1200	1500	1800	2100	2100	1800	1500	1200	900	600
64	HR_D10												
65													
66													
67													
68	RPM:	600	900	1200	1500	1800	2100	2100	1800	1500	1200	900	600
69	Alternate												
70													
71													
72													
73	RPM:	600	900	1200	1500	1800	2100	2100	1800	1500	1200	900	600
74	Ref validate												
75													
76													
77													

Figure B.7: Full test schematic

C

Timeplan

To create a rough plan for the project, a Gantt chart is established and shown in Figure C.1. This schedule is subject to change as the project evolves. The big, already known deadlines are listed below:

- W606/607- Planning-report hand-in.
- W622 - Written opposition.
- W622 - Oral presentation and defense of project.
- 2026/06/07 - Finished report hand-in.

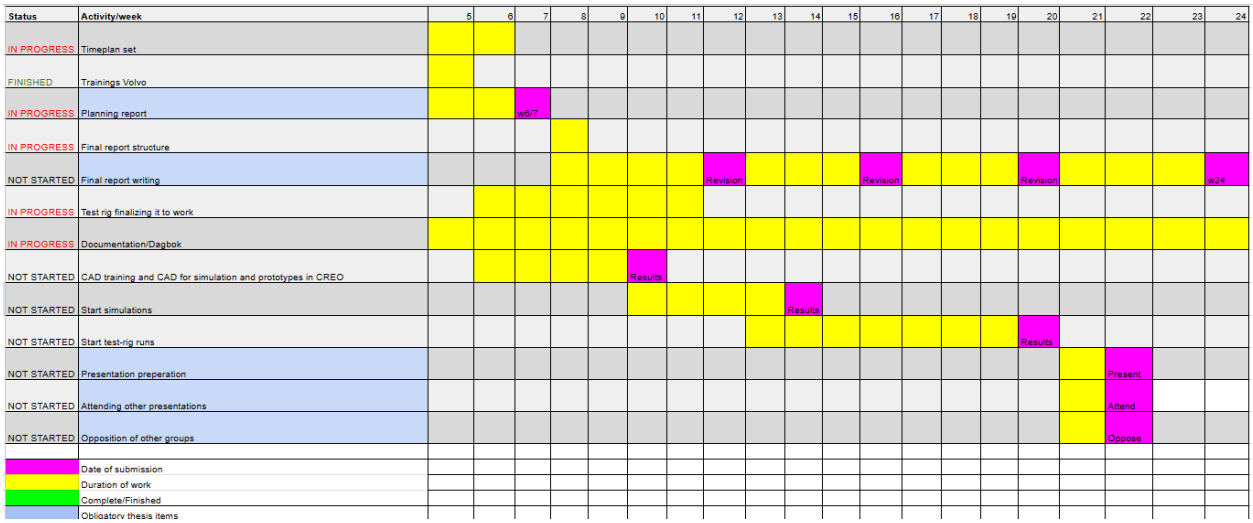


Figure C.1: Gantt schedule

One important success factor, is to start testing with the test-rig as soon as possible. It is set to start W12 (see above) at the latest, but the aim should be to start even earlier. This is to get rough testing results early and have time for adjustments, as well as accounting for unforeseen problems with the rig that can halt operation. The main focus of the project is the testing, as previously mentioned.

MECHANICS AND MARITIME SCIENCES
CHALMERS UNIVERSITY OF TECHNOLOGY
Gothenburg, Sweden
www.chalmers.se



CHALMERS
UNIVERSITY OF TECHNOLOGY